Chapter 10
Sensor Design

Jacqueline Rausch, Thorsten A. Kern and Christian Hatzfeld

Abstract Multiple sensors are applied in haptic devices designs. Even if they are not closed-loop controlled in a narrow sense of force or torque generation, they are used to detect movement ranges and limits or the detection of the presence of a user and its type of interaction with an object or human–machine interface (HMI). Almost any type of technical sensor had been applied in the context of haptic devices. Especially, the emerging market of gesture-based user interaction and integration of haptics due to ergonomic reasons extends the range of sensors potentially relevant for haptic devices. This chapter gives an introduction in technologies and design principles for force/torque sensors and addresses common types of positioning, velocity, and acceleration sensors. Further, sensors for touch and imaging sensors are addressed briefly in this section.

10.1 Force Sensors

Jacqueline Rausch

This section deals with selection and design of force sensors, which are implemented in haptic systems. Approaches like measuring current in actuators to derive occurring force are not part of the chapter. In Sect. 10.1.1, fundamental problems are discussed, which are the basis of every sensor design process. A selection of factors

J. Rausch (✉)
Roche Diagnostics GmbH, Sandhofer Straße 116, 68305 Mannheim, Germany
e-mail: j.rausch@hapticdevices.eu

T.A. Kern
Continental Automotive GmbH, VDO-Straße 1, 64832 Babenhausen, Germany
e-mail: t.kern@hapticdevices.eu

C. Hatzfeld
Institute of Electromechanical Design, Technische Universität Darmstadt,
Merckstr. 25, 64283 Darmstadt, Germany
e-mail: c.hatzfeld@hapticdevices.eu

C. Hatzfeld and T.A. Kern (eds.), *Engineering Haptic Devices*,
Springer Series on Touch and Haptic Systems, DOI 10.1007/978-1-4471-6518-7_10

to be taken in account is made in Sect. 10.1.1.5. After a short introduction in basic transfer properties, sensor characteristics are analyzed according to haptic aspects and complemented by application examples.

10.1.1 Constraints

The topology of haptic systems significantly influences force sensor design. The application of the haptic device itself has an extraordinary relevance. All systems have in common that an user mechanically contacts objects. It has to be clarified, which use of the device is intended, e.g., if it is going to be a telemanipulator for medical purposes, or a CAD tool with force feedback. The mechanical properties of the user itself, and in case of telemanipulation systems the mechanical properties of manipulating objects, have to be analyzed for the sensor development. All these factors will be discussed within this section.

10.1.1.1 Topology of the Device

The application itself appoints the topology of the haptic device. Taking control engineering aspects into account haptic systems can be classified into four types, which are discussed in Chap. 6. In the following, these topologies are analyzed referring to the measured values:

- Open-loop control of impedance: Measurement of user movements (velocity or displacement)and feedback of a force
- Closed-loop control of impedance: Measurement of both user movements and interaction and feedback of a force
- Open-loop control of admittance: Optional measurement of user force and feedback of a position
- Closed-loop control of admittance: Measurement of both user force and movements and feedback of a position

In case of open-loop control only the mechanical properties of objects have to be taken into account for force sensor design, independent if objects are physical or virtual ones. In case of haptic simulators like flight simulators, virtual objects are acting. Mechanical properties are often stored in look-up tables and force sensors are dispensable. In case of telemanipulation systems, the end effector of the haptic system interacts with physical objects. Their mechanical properties have to be detected with capable force sensors.

Most telemanipulation systems are impedance controlled. In case of closed-loop control, the mechanical impedance of both user and manipulating object are considered. In designing closed-loop impedance-controlled systems force sensors have to be integrated into the device detecting the user force. In designing closed-loop admittance-controlled systems the output movements of the haptic interface have to be measured using a velocity sensor (see Sect. 6.2)

Consequently, the measuring object can be both the user itself and a real, physical object. Beside its mechanical properties, the modality of the interaction with haptic systems has to be analyzed to identify fundamental sensor requirements such as dynamic bandwidth, nominal load, and resolution. The main factors influencing the sensor design are both contact situation and objects' mechanical properties. In the following, they are analyzed by examining the mechanical properties and the texture of the objects' surface separately.

10.1.1.2 Contact Situation

It is necessary to distinguish between the user of the haptic system and the physical object due to different interaction modalities identifying mechanical properties. If the user is the "measuring object," interaction forces have to be measured. Universally valid conclusions concerning amplitude, direction, and frequency of the acting force cannot be done. Mechanical impedance depends on the manner of grasping the device, age, and gender of the user itself (Chap. 3). In Sect. 3.1.3, the manners of grasping are classified: power-grasps, precision-grasps, and touch-grasps. In case of power- and precision-grasps, finger or palm are used as counter bearing, which results in a high absolute value of force up to 100 N [12, 31] and a stiffer contact.

Additionally, the direction of the force vector has to be taken into account. Depending on application of the haptic device and the manner of grasping up to six degrees of freedom results three force components and sometimes three torques. Neglecting torques between user and device three components of force have to be measured. If the user is in static contact with the handheld device, measuring normal force components with respect to orientation of the contact plane is sufficient. If the user is exerting relative movements to the device, shear forces also occur and three components have to be measured.

Considering the frequency dependence of humans' haptic perception, both static and dynamic signal components have to be considered equally. The lower cutoff frequency of haptic devices tends to quasistatic action at almost 0 Hz, which may happen when a device is held without movement in free space. If the force signal is subject to noise or even the slightest drift, the haptic impression will be disturbed soon (compare perception thresholds in Sect. 2.1). Manner and preload of grasping affect the upper cutoff frequency of the sensor. In case of power- and precision-grasps, the absolute value of force achieves higher values which results in an upper cutoff frequency being $\ll$ 10,000 Hz. Values of about 300 Hz are sufficient (Sect. 2.1). Within contact grasps preload is much lower than before enabling high-frequency components to be transmitted directly to the skin up to a range of approximately 1,000 Hz.

In case of telemanipulation systems, the end effector interacts with a real, physical object. Assumptions made for the measuring object "user" can partially be transferred to this situation. Following NEWTON's law *actio et reactio*, the absolute value of force depends on intensity and way of interaction. Possible examples are compression and lift of objects with a gripper, or exploration with a stick. For telemanipulation systems in minimally invasive surgery, the absolute value of force ranges from 1 to 60 N

(comp. e.g., [76]). The most promising approach is given by analyzing the intended application within preliminary tests and derivation of a model. The dynamics of the interaction, especially of the upper cutoff frequency, is dominated by the mechanical impedance of the object itself, which will be described within the following section.

10.1.1.3 Mechanical Properties of Measuring Objects

As stated for the user in Chap. 3, the mechanical impedance of objects can be subdivided into three physical actions: elastic compliance n, damping d, and mass m. In case of rigid objects made of, e.g., metal or ceramics, the property of elasticity is dominant. Interaction between haptic systems and objects can be considered as a rigid contact. Consequently, the force signal includes high-frequency components. The upper cutoff frequency should take a value of minimum 1,000 Hz to make sure to cover all dynamics responsible for haptic perception. Soft objects, such as silicone or viscera have a viscoelastic material performance. Following KELVIN viscoelastic behavior can be simulated by a network made of elastic compliances n_i and damping elements d_i, such as masses m_i. Using such an equivalent network, dynamic effects like relaxation and creeping can be modeled (Figs. 10.1 and 10.2).

First of all the elasticity of measuring objects has to be investigated for designing a haptic sensor. An arithmetic example in Sect. 2.4.2 compares the different cutoff frequencies of materials. For soft materials such as rubber, upper cutoff frequency takes values below 10 Hz. During interaction with soft materials mainly low-frequency components appear. The upper cutoff frequency is defined by the interaction frequency of 10 Hz at maximum [36, 73, 86]. If the measuring object is a soft one with embedded rigid objects, like for example tumors in soft body tissue, an upper cutoff frequency of about 1,000 Hz should be realized. To get more precise information about frequency requirements, it can hardly be done without an analysis of the interaction object. For a first rule of thumb calculated cutoff frequency as derived in Sect. 2.4.2 are sufficient. In case of doubt, the frequency range of the sensor should

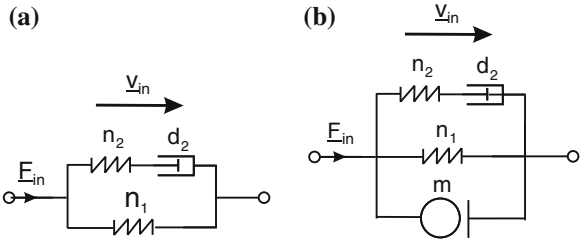

Fig. 10.1 Kelvin model (standard linear solid) modeling viscoelastic behavior of objects. For calculating the resonance frequency, a mass element has to be added. By adding further damping and spring elements, dynamic behavior of every object material can be modeled. **a** Kelvin model modeling dynamic effects. **b** Kelvin model extended by objects weight for calculating the resonance frequency

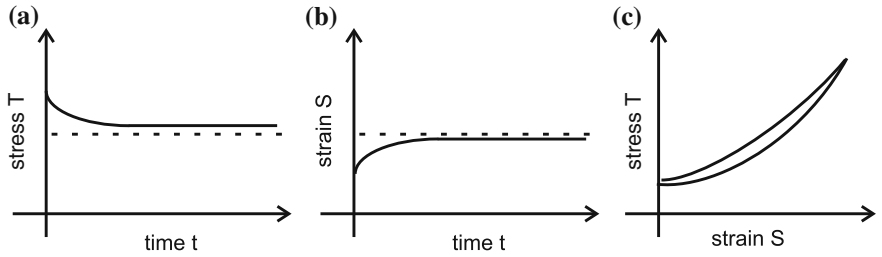

Fig. 10.2 Visualization of viscoelastic phenomena **a** relaxation, **b** creep, and **c** hysteris

always be oversized, not to already loose relevant haptic information at this very first point in the processing chain.

Beside dynamics, the required force resolution depends on a physiological value, too. The ↪JND lies in the range between 5 and 10 % of the absolute force value (Sect. 2.1). From the JND, the sensor characteristics of measurement uncertainty can be derived. If realized as a constant value—which is common to many technical sensor solutions—5 % of the lowest appearing value of force should be chosen to prevent distortion of the haptic impression of the object. Nevertheless, there is no actual requirement for haptic applications to have a constant or even linear sensor resolution. With telemanipulation systems, the interaction of the haptic system and real, physical objects is the main application. Depending on the type of interaction, frequently the surface structure of objects, the so-called texture becomes equally or even more important than the object's elastic compliance. Helpful literature for modeling dynamics of mechanical or electromechanical systems are [24, 47]. The resulting challenges for sensor development are discussed within the following section.

10.1.1.4 Texture of Measuring Objects

Properties, which are relevant for the human perception of texture, are geometrical surface structure on the one hand (e.g., the wood grain), on the other hand some kind of "frequency image" generated by the geometrical structure in the (vibro-)tactile receptors when being touched by skin. To detect the surface structure of an object, variation of force against the contact area can be derived. For **static measurement** sensor arrays of single-component force or pressure sensors are a common technical solution. These arrays are placed onto the object. The objects structure generates different values of contact forces, providing a force distribution on the sensor surface. Size of array and individual array elements cannot be defined in general, but depends on the smallest detectable structure on the measurement object itself. In case of static measurement sketched above, number and size of the sensor array elements should be dimensioned slightly smaller than the minimum structure of the measuring object. The size of each element may not be larger than half of the size of the smallest structure to be measured. However, even fulfilling this requirement aberration will appear. Figure 10.3 shows that in case of the width of the sensor element being larger

or identical to the smallest structure, the distance between the elements is detected smaller than in reality. With n sensor elements, the width of the structure element is replayed to $\frac{n+1}{n}$ and the distance to $\frac{n-1}{n}$. If the number of sensor elements per surface area increase, the aberration is diminishing and the structure is approximated more realistic (Fig. 10.4). However, with the number of elements, the effort of signal conditioning and analysis is increasing.

Beside the described aberration, an additional disadvantage of static measurements is given by the fact that the knowledge of the texture is not sufficient to get information about the object's material. The complete haptic impression needs frequency information depending on the elastic properties of texture and surface friction too. To gain these data, a relative movement between object and haptic system should be performed, to measure the texture **dynamically and spatially**. Depending on velocity of the relative movement and speed of the signal detection algorithms, the spatial resolution can be multiplied using the same number of sensor elements as in the example shown before. Even the use of sensor array with a simultaneous detection of multiple points becomes unnecessary. With knowledge about the exploration velocity and its direction, the information can be put into relation to each other. For texture analysis, multicomponent force sensors should be used, as especially the combined forces in the direction of movement and normal to the surface contribute to haptic perception [60]. This dynamic measurement principle is comparable with the intuitive exploration made by humans: To gain the texture of an object, humans gently touch and stroke over its surface. The surface structure excites the fingerprint to oscillate and the vibrotactile sensors acquire the frequency image. The absolute value of normal forces reached during such explorations are in a range of 0.3–4.5 N [13]. As stated earlier, force resolution is defined by the ↪JND. Haptic information about texture is included into the high-frequency components of the signal. For haptic

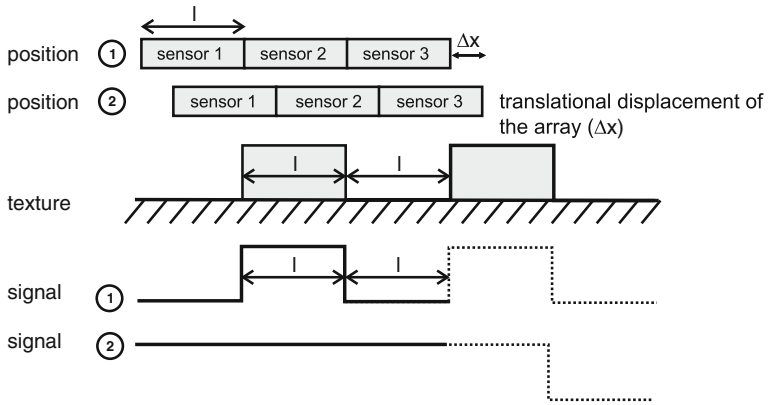

Fig. 10.3 Illustration of static and spatially resolved force measurement using as $3 \times n$ array. One sensing element has the same dimension like a texture element. At position 1 the array is optimally placed. If the array is shifted about Δx to position 2, the texture is incorrectly detected

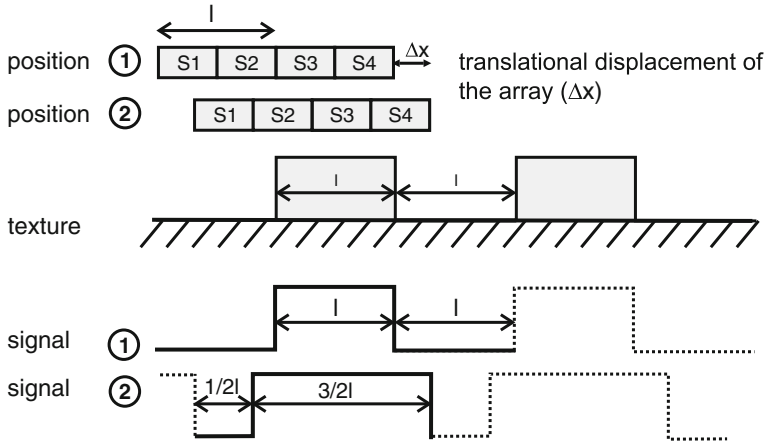

Fig. 10.4 Illustration of static and spatially resolved force measurement using as $6 \times n$ array. Size of one sensing element is half of a texture element. At position 1 the array is optimally placed. In case of any other position an aberration occurs. Aberration decreases with increasing number of sensing elements in an appropriate array

applications, the maximum frequency should be located at 1,000 Hz. The absolute value of nominal force should be chosen depending on the elastic compliance of the object. If the object is softer, the absolute value can be chosen lower as surface structures will deform and cannot be detected anymore. To be able to measure equally good at soft and rigid objects, the nominal force should take values $\leq$4.5 N. CALDWELL [13] for example decided to use $F = 0.3$ N.

10.1.1.5 Selection of Design Criteria

Following the description of the most relevant constraints, limiting factors for sensor design in haptic applications can be found in physiological values. Nominal force, force resolution, covered frequency range, and measurement uncertainty can be derived from humans' haptic perception. For a quantitative analysis of these requirements, the contact between measuring object and force sensor is to bring into focus. Measurement range and number of detectable force components are defined by the application and the structure of the device.

The geometrical dimensions and other mechanical requirements are given depending on the point of integration into the haptic system. The diagram displayed in Fig. 10.5 visualizes the procedure of how to identify most important requirements for sensor design.

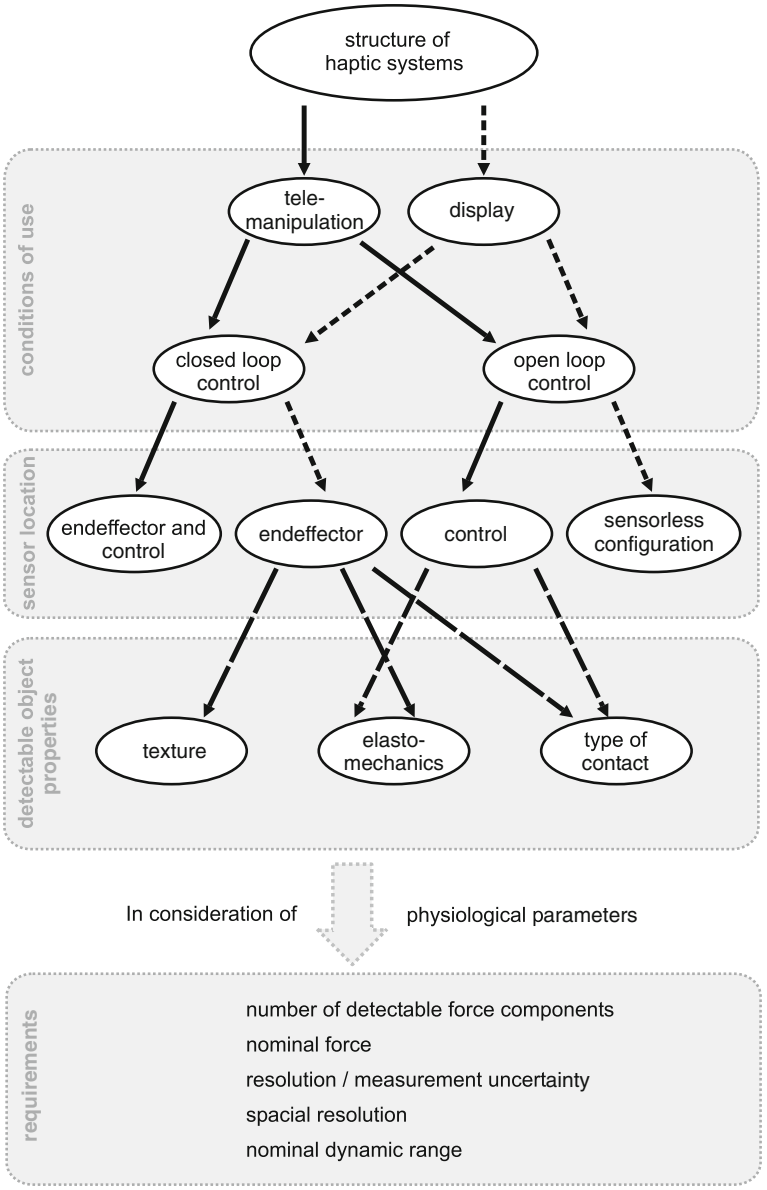

Fig. 10.5 Tree diagram to identify the principle requirements on haptic force sensors. Beside mechanical characteristics of the object physiological parameters of human haptic perception also have to be considered

10.1.2 Sensing Principles

Within the previous section, the most important criteria for the design and development of a haptic sensor were named and introduced. Section 10.1.3 summarizes major requirements once again in tabular form. In order to help choosing a suitable sensor principle, variants according to Fig. 10.6 are presented in this section. Beside established measurement elements, such as resistive, capacitive, optic, or piezoelectric ones, other less common sensor designs based on electroluminescence or active moving coils are discussed, too.

Most sensor principles are active transformers using the displacement principle for force measurement, which means that elastomechanic values such as stress or strain are detected and the corresponding force is calculated. Sensors belonging to the group of active transducers are resistive, capacitive, optic, and magnetic ones, working according to the displacement principle, too. Piezoelectric, electrodynamic, or electrostatic sensors are part of the group passive transducers. After a short introduction in elastomechanics, each sensing principle will be discussed according to its operating mode and several applications will be presented. All sensor principles will be estimated concerning their applicability for kinaesthetic and tactile force measurement, and put into relation to requirements known from Chap. 5. At the end of this chapter, a ranking method for the selection of suitable sensor principles is being given.

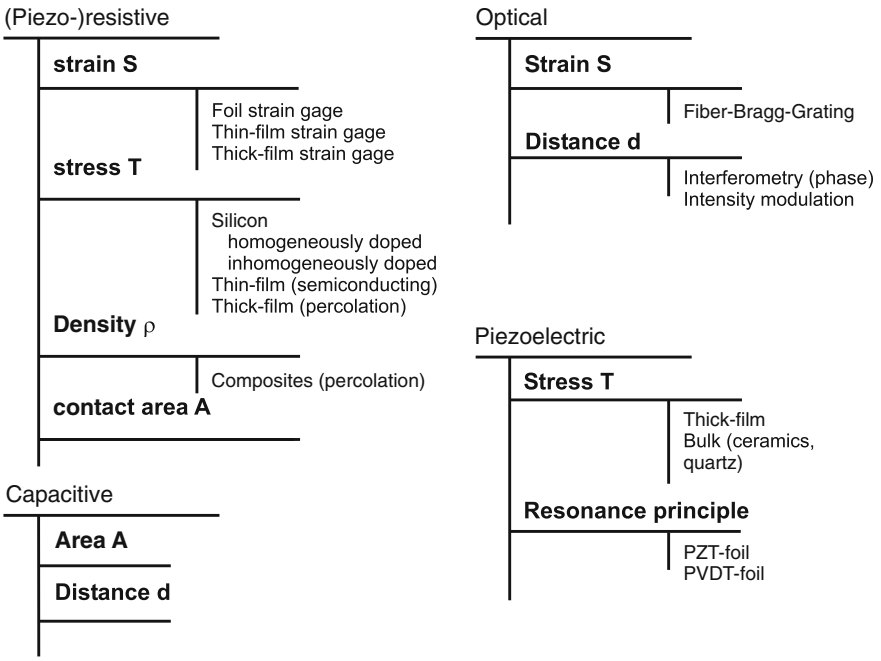

Fig. 10.6 Overview of established measurement principles for detecting forces in haptic systems. Furthermore, active sensor systems are also discussed in the following section

10.1.2.1 Basics of Elastomechanics

As mentioned before, large number of sensor principles are based upon elastomechanics. This section will summarize fundamental knowledge which is necessary for sensor design. If force is exerted to an elastic body, it deforms elastically depending on the amount of force. Internal stress T occurs resulting in a shape change—the strain S. Stress and strain are correlated with specific material parameters, the so-called elastic moduli s_{ij}.

For a better comprehension, a short *gedanken experiment* will be performed [28]. If a volume element ΔV is cut from an object under load (Fig. 10.7), substitute forces ΔF will act upon the surfaces of the cuboid to keep the state of deformation. Due to the required state of equilibrium, the sum of all forces and torques acting upon ΔV must equal zero.

Subdividing the force ΔF in its three components ΔF_1, ΔF_2, and ΔF_3, just those components remain orthogonal to the surface elements ΔA_j. The quotient of the acting force component ΔF_i and the corresponding surface element ΔA_j results in a mechanical stress T_{ij}. Following the equilibrium condition $T_{ij} = T_{ji}$, six independent tension components remain, resulting in the stress tensor. Tensor elements can be factorized into normal (stress parallel to surface normal) and shear stress components (stress orthogonal to surface normal). Analyzing the volume element ΔV before and after load, a displacement of the element ΔV with relation to the coordinate system $\langle 123 \rangle$ such as a deformation happens. The sides of the cube change their lengths and are not orthogonal to each other anymore (Fig. 10.8).

To describe that shape change, strain S_{ij} is introduced. The quantity strain is a tensor too, consisting of nine elements (Eq. 10.1)

$$\begin{pmatrix} d\xi_1 \\ d\xi_2 \\ d\xi_3 \end{pmatrix} = \begin{pmatrix} S_{11} & S_{12} & S_{13} \\ S_{21} & S_{22} & S_{23} \\ S_{31} & S_{32} & S_{33} \end{pmatrix} \cdot \begin{pmatrix} \Delta x_1 \\ \Delta x_2 \\ \Delta x_3 \end{pmatrix} \tag{10.1}$$

Due to volume constancy, the following correlation can be defined as

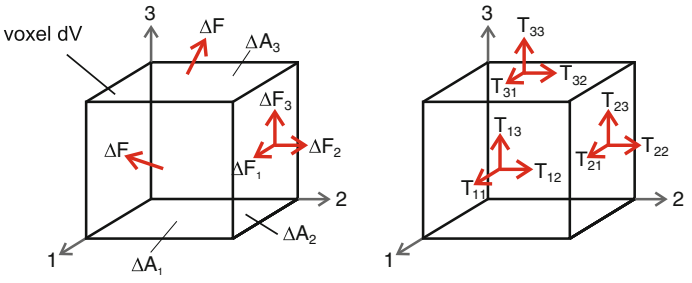

Fig. 10.7 Voxel dV of an elastic object. Due to external deformation, internal stress occurs which can be described by the component T_{ij} of the stress tensor [28]

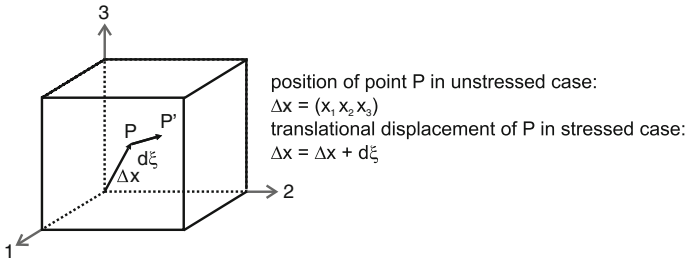

Fig. 10.8 Displacement of point P to P' due to application of force visualizes the state of strain [28]

$$S_{ij} = S_{ji} = \frac{1}{2} \cdot \left(\frac{\delta \xi_i}{\delta x_j} + \frac{\delta \xi_j}{\delta x_i} \right) \tag{10.2}$$

and thus, the matrix can be reduced to six linear independent elements. Normal strain components acting parallel to the corresponding normal surface result in volume change. Shear components, acting normal to the surface, describe the change of the angle between the borders of the volume element. In case of isotropic materials, such as metals or Al_2O_3 ceramics, the correlation between shape change mentioned before and after mechanical strains can be formulated as follows:

$$\begin{pmatrix} S_1 \\ S_2 \\ S_3 \\ S_4 \\ S_5 \\ S_6 \end{pmatrix} = \begin{pmatrix} s_{11} & s_{12} & s_{12} & 0 & 0 & 0 \\ s_{12} & s_{11} & s_{12} & 0 & 0 & 0 \\ s_{12} & s_{12} & s_{11} & 0 & 0 & 0 \\ 0 & 0 & 0 & 2(s_{11} - s_{12}) & 0 & 0 \\ 0 & 0 & 0 & 0 & 2(s_{11} - s_{12}) & 0 \\ 0 & 0 & 0 & 0 & 0 & 2(s_{11} - s_{12}) \end{pmatrix} \cdot \begin{pmatrix} T_1 \\ T_2 \\ T_3 \\ T_4 \\ T_5 \\ T_6 \end{pmatrix} \tag{10.3}$$

For simplification, six independent strains, respectively, stress components are summarized in a vector. Components with index 1, 2, and 3 mark normal components, those with indices 4, 5, and 6 mark shear components [28]. Parameters s_{ij} are regardless of direction. Taking YOUNGs modulus E and shear modulus G into account, parameters can be derived:

$$s_{11} = \frac{1}{E}, s_{12} = \frac{\nu}{E}, \frac{1}{G} = 2(s_{11} - s_{12}) = \frac{2}{E}(1 + 2\nu) \tag{10.4}$$

ν marks the so-called POISSON ratio, which is material dependent. Using metal ν values between 0.25 and 0.35 can be achieved. In case of homogeneous materials, Eq. (10.3) can be reduced to a linear correlation $T = E \cdot S$. For anisotropic materials such as silicon or quartz, elastomechanic properties depending on the orientation of the coordinate system ((comp. the following Sect. "Piezoresistive Silicon Sensors"), result in a matrix of elastic coefficients with up to 21 elements. For further reading on elastomechanics, e.g., [28, 105] are recommended.

Example "Beam Bending"

If a force vector is exerted to the tip of a beam bender made of isotropic materials and clamped on one side (Fig. 10.9), a bending moment M_B occurs.

Mechanical stress components $T(y)$ are linear distributed on the cross section and take values of $T(y) = c \cdot y$, whereas c is a proportional factor. Bending moment equals the integral of the stress $T_3(y)$ distributed on the cross section.

$$M_B = \int_A y \cdot T_3(y) \mathrm{d}A = c \cdot \int_A y^2 \mathrm{d}A \tag{10.5}$$

As the integral $\int_A y^2 \mathrm{d}A$ equals the axial moment of inertia I, c is calculated as

$$c = \frac{M_B}{I}. \tag{10.6}$$

The resulting strain components S_1 and S_2 act transversal to the beam's surface. For elastic deformation, strain component S_1 and stress component T_2 are correlated via the YOUNGs modulus E

$$S_2 = \frac{T_2}{E} = \frac{M_B}{I \cdot E} = \frac{F \cdot (l - z)}{I \cdot E} \tag{10.7}$$

and therefore depending on the geometry of the cross section A of the beam, position z at the beam's surface and acting force F. For calculations of strain component S_1 transversal contraction has to be considered as follows:

$$S_1 = -\nu \cdot S_2. \tag{10.8}$$

Further readings of elastomechanics, for example the calculations of deformation of fiber-reinforced composites, the works of GROSS [28], WERTHSCHÜTZKY [105], and BALLAS [4] are recommended.

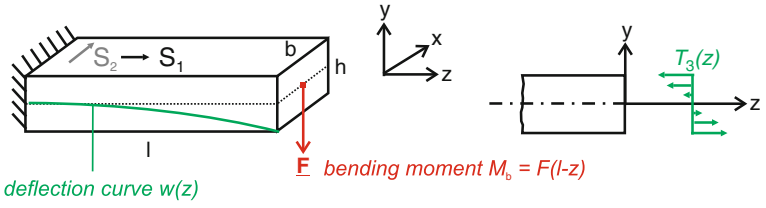

Fig. 10.9 Behavior of a bending beam, the *right-hand detail* shows stress distribution along the profile

10.1.2.2 Detection of Force

According to Fig. 10.9, acting forces can be measured evaluating both resulting strain distribution on the surface and displacement of beam. According to the example above, detection of strain S_2 can be derived using BERNOULLIs theory. Thus, strain components acting transversal to the surface can be neglected for slender and long-beam geometries. Stress- or strain-sensitive elements should be placed in such a way, that a maximum surface strain change can be detected.

Correlations described above are examples for a cantilever beam. Being able to measure more than just one force component, a suitable deformation element has to be designed considering the elastomechanic correlations. For example, works of BRAY [11] and RAUSCH [72] can help designing such an element. Primary objective is to generate a strain distribution in loading case, which enables to deduce the force components.

The correlation of force F_i and electric signal v_i of the sensor element usually is given by a linear system of equations (e.g., [104]). Equation (10.9) shows an example for a three-axial sensor:

$$\begin{pmatrix} v_1 \\ v_2 \\ v_3 \end{pmatrix} = \begin{pmatrix} a_{11} & a_{12} & a_{13} \\ a_{21} & a_{22} & a_{23} \\ a_{31} & a_{32} & a_{33} \end{pmatrix} \cdot \begin{pmatrix} F_1 \\ F_2 \\ F_3 \end{pmatrix} \tag{10.9}$$

It can be assumed that all force components contribute to each individual voltage signal v_i. The elements a_i of the matrix can be found by calibrating the sensor. During the calibration process, only one independent force component for each direction is applied to the sensor and the resulting voltage components are measured. After inverting the matrix $\mathbf{A}$ to $\mathbf{A}^{-1}$, the force vector can be calculated easily.

A lot of research is done in reducing the number of measuring cycles for calibration of multiaxial force sensors. Most common methods are:

- Least squares method [7]: Most accurate method. Execution of load cycle with n load steps for each direction. For a tri-axial force sensor $6n$ measuring cycles are necessary.
- Shape from motion method [39, 104]: Application of a force vector with known absolute value, which is randomly rotating in space. Accuracy comparable to the first method, but less time consuming. Only valid, if all components have the same amount of nominal load. If not so, then the third method is advisable.
- Hyperplane calibration method [62]: Accuracy and time consumption comparable to the second method. Three quasi-orthogonal load vectors must be applied to the sensor.

For further information on calibration check the above-mentioned literature.

10.1.2.3 Resistive Strain Measurement

One of the most commonly used sensing principles for force sensing is based on resistive detection of strain or rather stress components occurring in a (measuring) object. With resistive strain measurement, a resistor pattern is applied on the bending elements surface. Resistors must be located in areas of maximum strain. As a quick reminder: Electrical resistance is defined via

$$R_0 = \rho \cdot \frac{l}{A} = \rho \cdot \frac{l}{b \cdot h}, \tag{10.10}$$

ρ marks specific resistance, l, b, h (length, width, height) define volume of the resistor itself. The total differential shown in Eq. (10.11) gives relative resistivity change resulting from the deformation:

$$\frac{\mathrm{d}R}{R_0} = \underbrace{\frac{\mathrm{d}l}{l} - \frac{\mathrm{d}b}{b} - \frac{\mathrm{d}h}{h}}_{\text{rel. volume changing}} + \underbrace{\frac{\mathrm{d}\rho}{\rho}}_{\text{piezoresistive part}}. \tag{10.11}$$

Deformation causes on the one hand change the geometrical part $\frac{l}{A}$. Taking YOUNGs modulus E and POISSONs ratio ν account, plain stress for isotropic material can be derived [28]:

$$\frac{\mathrm{d}l}{l} = S_1 = \frac{1}{E} \cdot T_1 - \frac{\nu}{E} \cdot T_2, \tag{10.12}$$

$$\frac{\mathrm{d}b}{b} = S_2 = -\frac{\nu}{E} \cdot T_1 + \frac{1}{E} \cdot T_2, \tag{10.13}$$

$$\frac{\mathrm{d}h}{h} = S_3 = -\frac{\nu}{E} \cdot T_1 - \frac{\nu}{E} \cdot T_2. \tag{10.14}$$

Indices 1, 2, and 3 mark the direction components. Concerning the geometrical change, the resulting gage factor k describing the sensitivity of the material takes a value of about two (see Eq. 10.15). On the other hand, plane stress provokes a chance of specific resistivity ρ.

Material-specific changes will be discussed within Sect. "Piezoresistive Silicon Sensors." Using Eq. (10.15), the correlation between strain and relative resistivity change is formulated:

$$\frac{\mathrm{d}R}{R_0} = \underbrace{\left(2 - \frac{\mathrm{d}\,(N \cdot \mu)}{S \cdot N \cdot \mu}\right)}_{:=k,\ \text{gage factor}} \cdot S \tag{10.15}$$

whereas μ represents the electron mobility and N the number density of molecules. The change of the resistivity can be measured using a so-called WHEATSTONE bridge circuit. This circuit is built of one up to four active resistors connected in a bridge circuit and fed by a constant voltage or constant current (Fig. 10.10). Equation 10.16

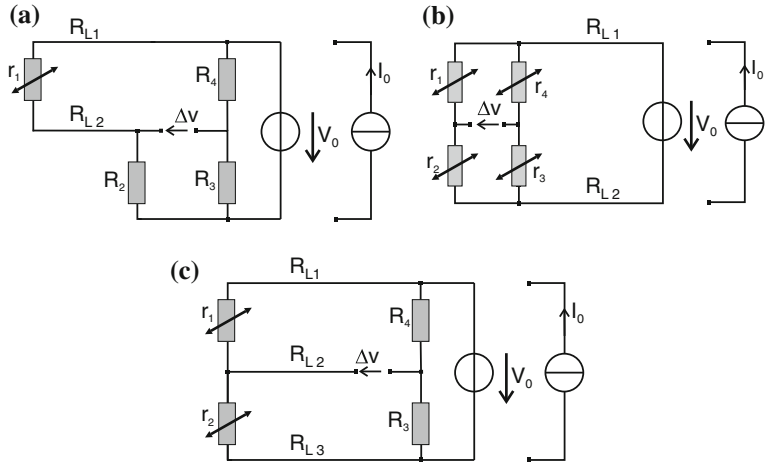

Fig. 10.10 WHEATSTONE bridge configurations for evaluating one up to four resistors. **a** Quarter bridge (1 active resistor). **b** Full bridge (4 active resistors). **c** Half bridge (2 active resistors)

calculates bridge Fig. 10.10c with the assumption that the basic resistances R_{0i} equal the resistance R_0. The values of R_0 such as gage factors are specific to material and listed in Table 10.1 (further informations e.g., [72, 81]).

$$\Delta v = \frac{V_{cc}}{R_0 \cdot I_0} = \frac{1}{4} \cdot \left\{ \frac{r_1}{R_{01}} - \frac{r_2}{R_{02}} + \frac{r_3}{R_{03}} - \frac{r_4}{R_{04}} \right\} \tag{10.16}$$

The supply with constant current I_0 has the great advantage that a temperature-dependent drift of the measurement signal will be compensated. More advanced information can be found in [20, 106].

In case of metallic resistors, a gage factor of approximately two occurs. The material-specific component of metals is less important and affects the first decimal place only. In case of semiconductors and ceramic materials, the material-specific component is dominant. In case of semiconductor-strain gages, the gage factor takes values up to 150. Using resistor pastes, applied in thick-film technology on substrates,[1] and polysilicon layers, sputtered in thin-film technology the material-specific component is dominant. On this, gage factors achieve values of up to 18 in case of thick-film resistors and up to approximately 30 for thin-film resistors. Table 10.1 lists the gage factor for several materials usually used in strain measurement. As mentioned earlier, strain gages are manufactured in different technologies. The most commonly used types are foil-strain gages; thick- and thin-film manufactured measurement elements are found mainly in OEM-sensors and for specific solutions in automation industry due to the necessary periphery and the manufactur-

[1] For substrate material mainly (layer-) ceramics are used. Less frequent is the use of metals, as isolating layers have to be provided then.

Table 10.1 Gage factor, strain resolutio,n and nominal strain of important resistive materials according to [72]

Technology	Material	Gage factor	R_0 in Ω	S_{min}	S_N (%)	References
Foil-strain gage	CuNi	About 2	120, 350, 700	$\pm 10^{-7}$	±0.1	[32, 35, 91]
Thick-film	$Bi_2Ru_2O_7$	12.1–18.3	1,000	$\pm 10^{-6}$	±0.1	[3, 65]
	PEDOT:PSS	0.48–17.8	–	≥ 10	–	[44, 46]
Thin-film	TiON	About 1k	4–5	$\pm 10^{-7}$	±0.1	[3, 42, 105]
	Poly-Si	20–30	About 1k	$\pm 10^{-7}$	±0.1	[3, 105]
Si-technology	Homogeneous	100–255	120–1k	$\pm 10^{-6}$	±0.2	[58]
	Inhomogeneous	80–255	1k–5 k	$\pm 10^{-7}$	±0.05	[5, 23, 105]
Fiber-sensors	Carbon	1.3–31	About 10 k	–	0.2–15	[16, 43]

ing process. Relevant literature can be found in the publications of PARTSCH [65] and CRANNY [18].

To deposit thin-film sensing layers, other technologies like inkjet or aerosoljet printing can be used. The inks are suspensions containing electrically conducting particles made of carbon, copper, gold, silver, or even conducting polymers like PEDOT:PSS. One advantage is that compared to conventional thick-film pastes, the finishing temperature is below 300 °C and thus various substrates can be functionalized. Further information can be found in [44, 49, 72].

Foil-strain gages are multilayer systems made of metallic measurement grids and organic substrates. It is applied (Fig. 10.11) and fixated on bending elements via cold hardening cyanoacrylate adhesive (strain analysis) or via hot hardening adhesives such as epoxy resin (transducer manufacture). These gages are long-term stable, robust, and especially used for high-precision tasks in wind-tunnel-scales and balance sensors. Achievable dynamics, resolution, and measurement range are solely depending on the deformation element. The minimum size of the individual strain gages taken of the shelf is in the area of 3 mm width and 6 mm length. The measurement pattern itself is smaller in its dimensions. On this, it is possible to shorten the organic substrate to finally achieve 1.5 mm width and 5 mm length as a typical min-

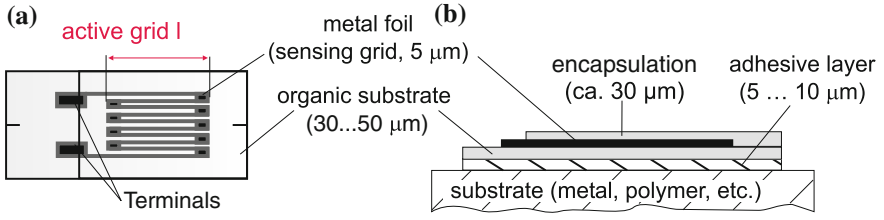

Fig. 10.11 Assembly of conventional strain gages: measuring grid is usually made of a patterned metal foil. In case of special applications, metal wires are applied. **a** Top view of strain gage. **b** Cross section of integrated gage

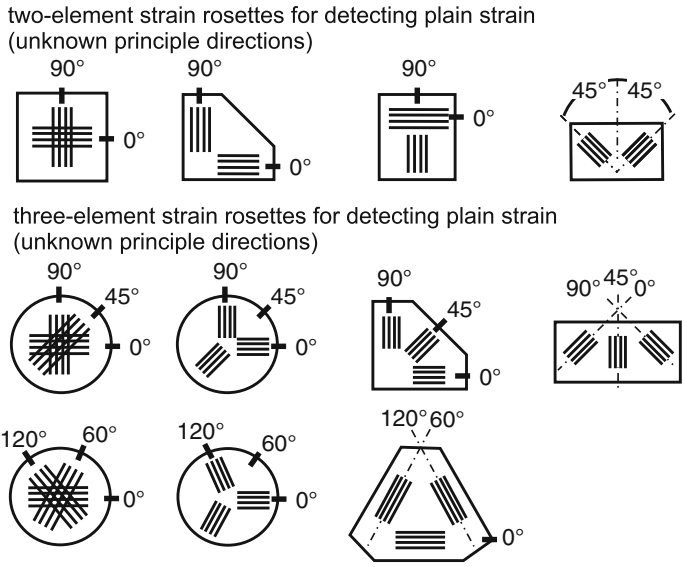

Fig. 10.12 Compilation of possible grid configurations of strain gages. See also [105]

imum size. If foil-strain gages are considered, the surface strains resulting from the nominal load should be 1,000 μm/m for an optimum usage of the strain gage. Many measurement pattern are applied for force and torque sensors. Figure 10.12 shows a selection of commercialized measuring grids ready for application on deformation elements.

Beside resistive foil-strain gages, semiconductor-strain gages are available. Their general design is comparable to conventional strain gages, as the semiconducting elements are assembled with organic substrates.[2] Measurement elements are used identical to foil-strain gages and are available in different geometrical configurations such as T-rosettes.

Using measuring elements with a higher gage factor (Table 10.1), deformation elements can be designed stiffer, allowing smaller nominal strains. Such elements are especially relevant for the design of miniaturized sensors for haptic systems, as small dimensions and high cutoff frequencies have to be achieved. A commercially available example is the OEM-sensor *nano 17* from ATI (Fig. 10.13). Strain elements are piezoresistive ones and their gage factor takes values of approximately 150. Due to high potential for miniaturization and manifold application in haptic systems, piezoresistive sensors—especially silicon sensors—will be discussed in an independent subsection.

[2] Also single semiconducting elements without organic substrate are available. They are highly miniaturized (width of about 230 μm, length of about 400 μm), but has to be insulated from the deformation element.

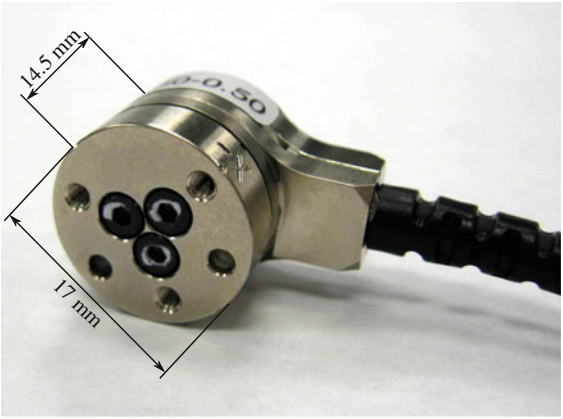

Fig. 10.13 Miniaturized force/torque sensor nano17 (*ATI Industrial Automation, Inc.*, Apex, NC, USA). Resonance frequency of the sensor takes a value of about 7.2 kHz

Piezoresistive Silicon Sensors

Published by SMITH in 1954 for the first time [89], semiconducting materials with a symmetric crystal structure such as silicon or germanium possess a change in their conductivity σ due to an applied force or pressure. In the following paragraphs, this effect is discussed more deeply for monocrystalline silicon.

The Piezoresistive Effect

If a semiconducting material is deformed due to a load, stress components T_i are generated inside the material. For your information: Due to the anisotropic properties of the material, the elastomechanic properties are depending on the position of the coordinate system, and consequently on the orientation of the crystal lattice. These stress components affect the electron mobility μ and—as a consequence—the specific resistivity ρ. ρ is a material-specific value, characterized via the parameters electron mobility μ and number of charge carriers N (comp. Sect. 10.1.2.1). Considering these parameters, correlation between relative resistivity change and the resulting strain tensor can be expressed to:

$$\frac{\mathrm{d}\rho}{\rho} = \frac{\mathrm{d}V}{V} - \frac{\mathrm{d}(N \cdot \mu)}{N \cdot \mu}, \quad \text{with } \rho = \frac{V}{N \cdot \mu \cdot |q|}, \tag{10.17}$$

whereas V is the volume of the resistive area, and $|q|$ is the charge of the particles.

Following the OHM's law the specific resistance ρ is connected by the vector $\mathbf{E} = (E_1; E_2; E_3)^T$ of the electrical field and the current density $\mathbf{J} = (J_1; J_2; J_3)^T$:

$$\begin{pmatrix} E_1 \\ E_2 \\ E_3 \end{pmatrix} = \begin{pmatrix} \rho_{11} & \rho_{12} & \rho_{13} \\ \rho_{21} & \rho_{22} & \rho_{23} \\ \rho_{31} & \rho_{32} & \rho_{33} \end{pmatrix} \cdot \begin{pmatrix} J_1 \\ J_2 \\ J_3 \end{pmatrix} = \begin{pmatrix} \rho_1 & \rho_6 & \rho_5 \\ \rho_6 & \rho_2 & \rho_4 \\ \rho_5 & \rho_4 & \rho_3 \end{pmatrix} \cdot \begin{pmatrix} J_1 \\ J_2 \\ J_3 \end{pmatrix} \tag{10.18}$$

Due to the symmetric crystalline structure of silicon,[3] six independent resistive components ρ_i result, which are symmetrical to the diagonal of tensor ρ. Taking the matrix of piezoresistive coefficients π into account, the influence of the six acting stress components T_i can be formulated. The cubic symmetry results in reduction of the number of piezoresistive and direction-dependent coefficients to three. By doping silicon with impurity atoms such as boron or phosphor areas of higher resistivity are generated. By influencing the type and the concentration of dopant, the three π-coefficients can be influenced. Further information on doping can be found, e.g., in [5, 6].

$$\begin{pmatrix} \rho_1 \\ \rho_2 \\ \rho_3 \\ \rho_4 \\ \rho_5 \\ \rho_6 \end{pmatrix} = \begin{pmatrix} \rho_0 \\ \rho_0 \\ \rho_0 \\ 0 \\ 0 \\ 0 \end{pmatrix} + \begin{pmatrix} \pi_{11} & \pi_{12} & \pi_{12} & 0 & 0 & 0 \\ \pi_{12} & \pi_{11} & \pi_{12} & 0 & 0 & 0 \\ \pi_{12} & \pi_{12} & \pi_{11} & 0 & 0 & 0 \\ 0 & 0 & 0 & \pi_{44} & 0 & 0 \\ 0 & 0 & 0 & 0 & \pi_{44} & 0 \\ 0 & 0 & 0 & 0 & 0 & \pi_{44} \end{pmatrix} \cdot \begin{pmatrix} T_1 \\ T_2 \\ T_3 \\ T_4 \\ T_5 \\ T_6 \end{pmatrix} \cdot \rho_0 \tag{10.19}$$

For homogenous silicon with a small concentration of dopants, the values in Table 10.2 can be used.

Depending on angle between current density vector $\mathbf{J}$ and stress component T_i, three effects can be distinguished. Within the so-called longitudinal effect current i is guided parallel to the normal component of stress, within transversal effect i is guided normal to the normal component of stress, and thus shear effect i is guided parallel or normal to the shear component of stress. Figure 10.14 visualizes the mentioned correlations.

For the resistivity change, depending on the orientation of the resistive area from Fig. 10.14, the following equation becomes valid:

$$\frac{\mathrm{d}R}{R} \approx \frac{\mathrm{d}\rho}{\rho} = \pi_\mathrm{L} \cdot T_\mathrm{L} + \pi_\mathrm{Q} \cdot T_\mathrm{Q} \tag{10.20}$$

Table 10.2 Piezoresistive coefficients of homogeneously doped silicon [5]

Doping	N in $\frac{1}{\mathrm{cm}^{-3}}$	ρ in Ω cm	π_{11} in $\frac{\mathrm{mm}^2}{N}$	π_{12} in $\frac{\mathrm{mm}^2}{N}$	π_{44} in $\frac{\mathrm{mm}^2}{N}$
n-Si	6×10^{14}	11.7	-102.2×10^{-5}	$+53.4 \times 10^{-5}$	-13.6×10^{-5}
p-Si	1.8×10^{14}	7.8	$+6.6 \times 10^{-5}$	-1.1×10^{-5}	$+138.1 \times 10^{-5}$

[3] Face centered cubic.

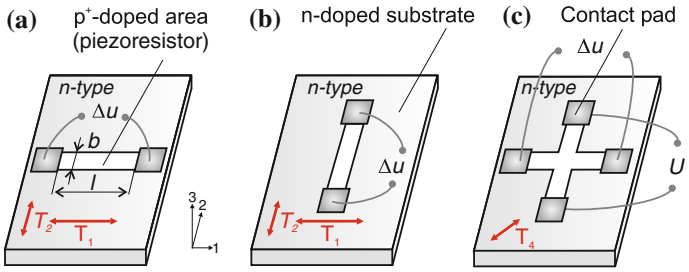

Fig. 10.14 Visualization of the piezoresistive effects: longitudinal, transversal, and shear effect in silicon [72]. Transversal and longitudinal effect is normally used for commercial silicon sensors **a** longitudinal effect ($T_1 \| J \rightarrow T_1 = T_L$), **b** transversal effect ($T_1 \perp J \rightarrow T_1 = T_Q$), **c** shear effect (piezores. Hall effect)

Table 10.3 Compilation of π_l- und π_q-coefficients for selected resistor assemblies dependent on the crystallographic orientation [90]

Surface orientation	Longitudinal	π_l	Transversal	π_q
(100)	[100]	π_{11}	[010]	π_{12}
	[110]	$\frac{\pi_{11}+\pi_{12}+\pi_{44}}{2}$	$[\bar{1}10]$	$\frac{\pi_{11}+\pi_{12}-\pi_{44}}{2}$
(110)	[111]	$\frac{\pi_{11}+2\pi_{12}+2\pi_{44}}{3}$	$[\bar{1}\bar{1}2]$	$\frac{\pi_{11}+2\pi_{12}-\pi_{44}}{3}$
	[110]	$\frac{\pi_{11}+\pi_{12}+\pi_{44}}{2}$	[001]	$\frac{\pi_{11}+5\pi_{12}-\pi_{44}}{6}$

As a consequence, longitudinal and transversal stress components are influencing the calculation of the resistivity change. Depending on the crystallographic orientation of the resistive areas the π-coefficient is formed by longitudinal and transversal coefficient (Table 10.3). For homogeneous Boron concentration of $N_R \approx 3 \times 10^{18}\,\mathrm{cm}^{-3}$ the following values are achieved [5]:

$$\pi_L = 71.8 \times 10^{-5}\,\mathrm{MPa}^{-1},$$

$$\pi_Q = -65.1 \times 10^{-5}\,\mathrm{MPa}^{-1}.$$

More advanced information for the design of piezoresistive silicon sensors can be found in the publications of BAO [5], BARLIAN [6], MEISS [53], RAUSCH [72] and WERTHSCHÜTZKY [68].

Examples of Piezoresistive Silicon Sensors

Piezoresistive silicon sensors for physical quantities like pressure and force are commonly integrated in silicon deformation elements. In case of pressure transducers, this kind of manufacture is state-of-the-art. For all pressure ranges sensor elements

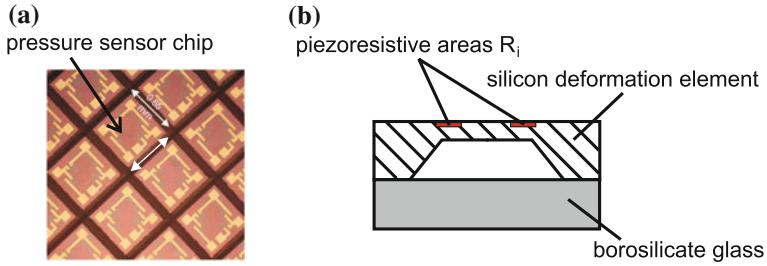

Fig. 10.15 Example of piezoresistive silicon-pressure sensors [88], **a** unseperated chips, edge length of about 650 μm, **b** sectional drawing of the sensor

can be purchased. For example, the company *Silicon Microstructures Inc. (SMI)* sells chips with glass counterbody for absolute pressure measurement with an edge length of 650 μm (Fig. 10.15a). In case of suitable packaging, these sensors could be arranged in an array to measure the uniaxial force- or pressure-distribution on a surface.

In case of force sensors, realization of miniaturized multicomponent force sensors is the current issue in research. Dimensions of single sensor elements range from 200 μm to 2 mm. Nominal force covers a range of 300 mN to 2 N. Due to batch-manufacture of measurement elements, realization of both single sensor elements and array-design[4] is possible. Sensitivity of sensors takes values of 2 % relative resistivity change in loading case. Figure 10.16 shows four examples of current topics in research. Variants (a) [100], (b) [103], and (d) [52] were designed for force measurement in haptic systems. Variant (c) [10] was built for tactile, dimensional measurement technology. Force transmission is always realized by beam- or rod-like structures.

Since 2007, a Hungarian manufacturer is selling the *Tactologic* system. Up to 64 miniaturized sensor elements are connected in an array of $3 \times 3\,\text{mm}^2$. Sensor elements have a size of $0.3 \times 0.3\,\text{mm}^2$ and are able to measure shear forces up to 1 N and normal force up to 2.5 N at nominal load. The force transmission is realized by soft silicone dots, applied to every individual sensor element (Fig. 10.17a, b). Using this array, static and dynamic loads in the range of kilohertz are measurable. But the viscoelastic material properties of the force transmission influence the dynamics due to creeping, especially the measurement of the normal forces [101, 102]. Another approach is to use piezoresistivity of silicon micromachined transistors using the above-mentioned shear effect (especially MOSFET, see [21, 40, 99]). As well as strain measurement these sensors are used to monitor the state of stress occurring in packaging process [21, 99]. Polyimide foil containing sensor elements (strain-sensitive transistors) with a thickness of about 10 μm are available since at least around year 2000 [40].

[4] By isolating arrays instead of single sensors in the last processing step.

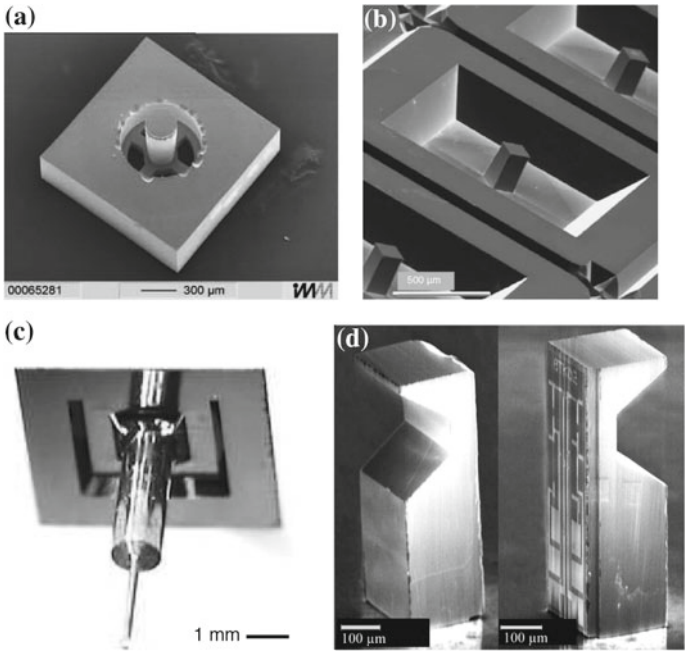

Fig. 10.16 Different realizations of piezoresistive silicon force sensors: **a** [100], **b** [103], **c** [10], and **d** [52]; **a** Single tri-axial sensor. **b** Array of tri-axial sensors. **c** Single tri-axial sensor. **d** Single tri-axial sensor [52]

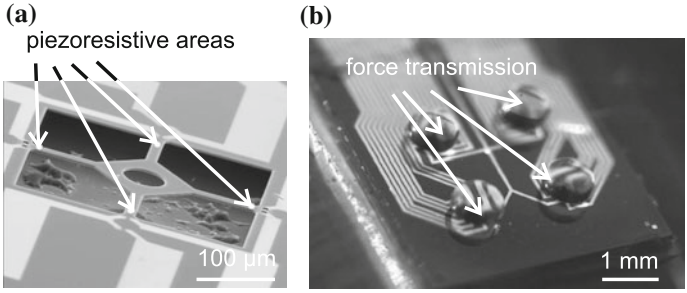

Fig. 10.17 Tactile multicomponent force sensor [101]. **a** One taxel of the sensing array (Tactologic), **b** 2 × 2 array for triaxial-force measurement (Tactologic)

Further Resistive Sensors

Besides resistive transducers presented until now, other more "exotic" realizations exist, which will be introduced within three examples. All sensors are suitable for array assembly to measure position-dependent pressure and a single-force component. The used measurement principles are based on the change of geometrical parameters of the force elements. The examples shown in Fig. 10.18a and b [41, 78]

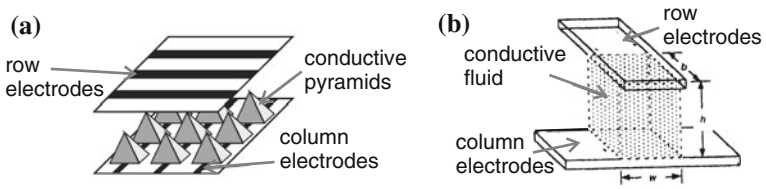

Fig. 10.18 Selected examples of foil sensors using the effect of a load-dependent constriction resistance. **a** Micromachined tactile array developed by Fraunhofer Institute IBMT. **b** Variation of the electrodes distance [41, 78]

use the load-dependency of the constriction resistance. With increased pressure,[5] the electrical contact area A increases and the resistance decreases.

The companies *Interlink Electronic* and *TekScan* use this effect for their sensor arrays (also called *Force Sensing Resistors—FSR*) (Fig.10.19). Interlink distributes polymer foils printed with resistor pastes in thick-film technology. Their basic resistance takes values in the region of $M\Omega$. The sensor foils have a height of 0.25 mm and a working range of zero to one Newton, respectively, 100 N. Beside the sensitivity to force or pressure, the sensors show a temperature dependency of 0.5 % K.

The sensor foils from *TekScan* are located in the range of 4.4 up to 440 N, the spatial distribution reaches up to 27.6 elements per centimeter. The available array size reach from approximately $13 \times 13\,\text{mm}^2$ up to $0.5 \times 0.5\,\text{m}^2$. The height of the foils is around 0.1 mm. The measurement inaccuracy takes a value of 10 %. The frequency range reaches from static up to 100 Hz. Beside the application in data gloves, as described by BURDEA [12], the foil sensors are used in orthopedics to detect the pressure-distribution in shoes and prosthesis and within automotive industry for ergonomic studies.

Another approach is the variation of the distance between two electrodes (see Fig. 10.18b). The sensing element is made of flexible substrates. The electrodes are arranged in rows and columns. The gaps in between are filled with an electrical

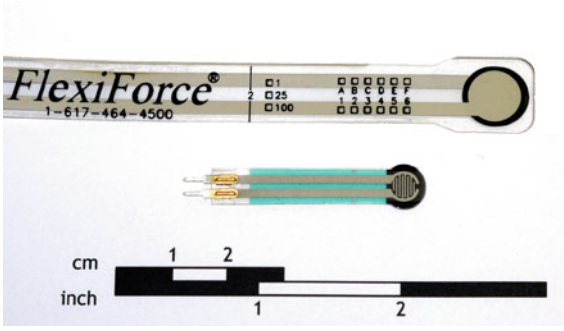

Fig. 10.19 Foil sensors for compressive force detection, *top* FLEXIFORCE by *TekScan Inc.*, South Boston, MA, USA, *bottom* FSR by *Interlink Electronics*, Camarillo, CA, USA. These sensors are often used to detect grasp forces, for example

[5] The force can be calculated taking the contact area into account.

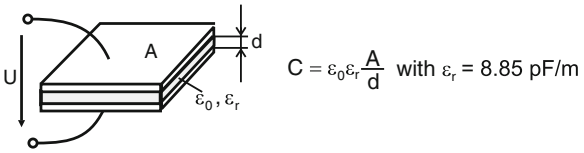

Fig. 10.20 Assembly of a single capacitance

conductive fluid. In loading case, the fluid is squeezed out and the distance of the electrodes varies. A disadvantage of this principle is given by the necessity for very large distance variations up to 10 mm to achieve usable output signals. Until today, this principle is still a topic of research.

10.1.2.4 Capacitive Sensors

Within every capacitive sensor at least two electrodes are located parallel to each other. Figure 10.20 shows a design based on a single measurement capacity. In contrast to the resistive principle—measuring the mechanical variables stress and strain—the capacitive principle measures the integral values displacement (or elongation) directly.

Concerning the working principle, three classes can be identified, which shows some similarities to electrostatic actuators discussed in Sect. 9.5. The first class uses the displacement principle. On this, the mechanical load changes the electrode distance d or the active electrode area A. In the third class, the relative dielectric ε_r is influenced. The change of electrode distance is usually used for measuring force, pressure, displacement, and acceleration. In these cases, the mechanical load is directly applied to the electrode and displaces it relatively to the other one. The resulting capacitance change can be calculated:

$$\frac{\Delta C}{C_0} = \frac{1}{1 \pm \xi/d} \approx \pm\frac{\xi}{d}. \tag{10.21}$$

ξ marks the change of distance. Additionally, the electrode distance can be kept constant, and only one electrode can be parallel displaced (Fig. 10.21). The active electrode area varies accordingly and the resulting capacitance change can be used to measure angle, filling level, or displacement. It is calculated according to:

$$\frac{\Delta C}{C_0} = 1 \pm \frac{\Delta A}{A_0}. \tag{10.22}$$

The third option for a capacitance change is the variation of the relative dielectric. This principal is often used for measuring a filling level, e.g., of liquids, or as a proximity switch for layer thickness. This capacitance change is calculated according to

$$\frac{\Delta C}{C_0} = 1 \pm \frac{\Delta \varepsilon_r}{\varepsilon_{r0}}. \tag{10.23}$$

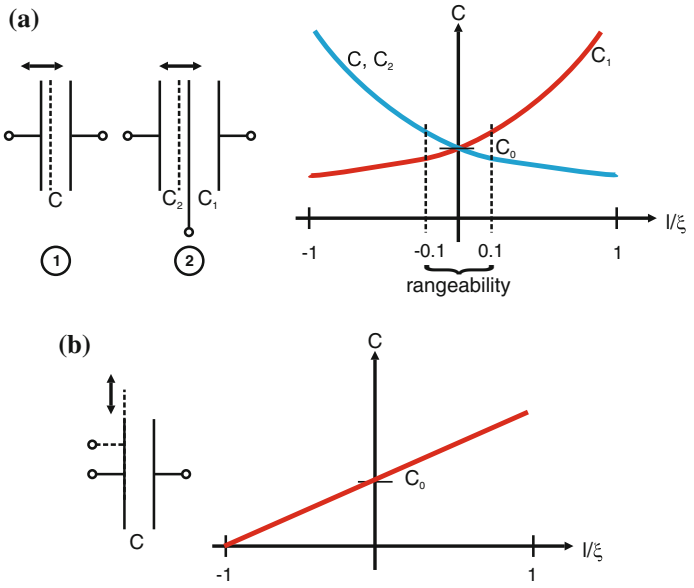

Fig. 10.21 Schematic view of capacitive sensing principle and characteristic curve of capacitance. **a** Variation of electrode distance in case of single (*1*) and differential setup (*2*). **b** Variation of effective electrode area

Characteristics of Capacitive Pressure and Force Sensors

The main principle used for capacitive force, respectively, pressure transducers is measuring displacements. Consequently, the following paragraph will concentrate on this principle. As stated within Eq. (10.21) for the change of distance, the interconnection between capacitance change and mechanical load is nonlinear for single capacities. The displacement ξ lies in the range of 10 nm to 50 µm [105]. For linearization of the characteristic curves, an operating point has to be found, e.g., by arranging three electrodes as a differential capacitor. The displacements ξ typical for the working range are $\leq$10 % than the absolute electrode distance d. In this range, the characteristic curve can be approximated as linear (Fig. 10.21a). With the principle varying the electrode's surface the capacitance changes proportional to it, resulting in a linear capacitance change (Fig. 10.21b).

The evaluation of the capacitance change can be made by an open- or closed-loop measuring method. Concerning open-loop method, the sensor is either integrated in a capacitive bridge circuit, or it is put into a passive oscillating circuit with coil and resistor. Alternatively, the impedance can be measured at a constant measurement frequency. An alternative could be the application of a pulse-width-modulation (also called: recharging method). A closed-loop approach is characterized by the compensation of the displacement by an additional energy. The main advantage of the closed-loop signal conditioning is the high linearity achieved by very small displacements. Additional information can be found in [105, 106].

The advantage of capacitive sensor in contrast to resistive sensors lies in the effect of little power consumption and high sensitivity. Additionally, the simple structure enables a low-cost realization of miniaturized structures in surface micromachining (Fig. 10.22). In contrast to the resistive sensors—where positions and dimensions of the resistive areas have a direct influence on transfer characteristics—the manufacture tolerances for capacitive sensors are quite high. Mechanically induced stress due to packaging and temperature influence has almost no influence on their performance. Even mispositioning of electrodes next to each other do not change the transfer characteristics, only the basic capacitance. The manufacturing steps with silicon capacitive sensors are compatible to CMOS-technology. This allows a direct integration of the sensor electronics on the chip, to minimize parasitic capacities. Especially with miniaturized sensors,[6] a good signal-to-noise ratio can be achieved [71]. The problem of parasitic capacities or leakage fields is one of the major challenges for the design of capacitive actuators, as it achieves easily a level comparable to the capacitance used for measurement. An additional challenge can be found in the constancy of the dielectric value, which is subject to changes in open-air gap actuators due to humidity or other external influence factors.

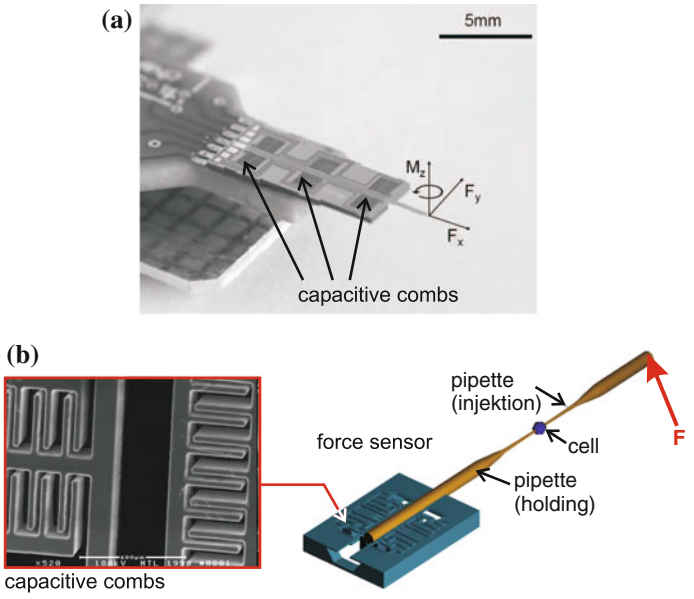

Fig. 10.22 Examples of capacitive silicon multicomponent force sensors. **a** 2-component force sensor, nominal load 1.5 mN [8], **b** 6-component force/torque sensor, nominal load 500 μN [93]

[6] Due to the small electrodes a small basic capacitance is achieved, comp. equation in Fig. 10.20.

Examples of Capacitive Sensors

Concerning the manufacturing technology, capacitive sensors integrated in haptic systems can be distinguished in three classes. The first class is represented by miniaturized pressure sensors, being realized using silicon microtechnology. Due to their small size of few millimeters, the moving masses of the sensor are low and thus cover a wide dynamic range (frequencies from static to several kilohertz). As shown before, the micromachined capacitive sensors may be combined to arrays for measuring spatially distributed load. As an example, SERGIO [85] reports the realization of a capacitive array in CMOS-technology. A challenge is given by the capacity changes in the range of femto-Farad, which is similar to the capacity of the wiring. A relief is given by a parallel circuit of several capacities to a sensor element [105]. The frequency range of the shown examples range from static measurement up to several MHz upper cutoff frequency. Consequently, it is suitable for haptic-related measurements of tactile information. Another example is given by an array made of polysilicon. It has an upper cutoff frequency of 1,000 Hz and a spatial resolution of 0.01 mm^2 suitable for tactile measurements. It was originally designed for acquisitions of fingerprints. REY [75] reports the use of such an array for intracorporal pressure measurement at the tip of a gripper. Once again the leakage capacities are a problem, as they are within the range of the measured capacity changes.

Two examples of multicomponent force sensors built in surface micromachining are shown in Fig. 10.22a, b [8, 93]. The two-axial sensor[7] is designed for atomic force microscopy. The nominal load of this application lies in a range of μN. The three-axial sensor was designed for micromanipulation, e.g., in molecular biology, with similar nominal values of several μN. Both sensors are using the displacement change for measurement.

The second class is represented by ceramic pressure load cells. They are widely used in automotive industry and industrial process measurement technology. Substrate and measurement diaphragm are typically made of Al_2O_3 ceramics. The electrodes are sputtered on ceramic substrates. Substrate and measurement diaphragm are connected via solder applied in thick-film technology. In contrast to silicon sensors, ceramic sensors are macroscopic and have dimensions in the range of several centimeters. Based on the technology sensors in differential-, relative-, and absolute-designs with nominal pressures in the range of zero to 200 mbar such as in zero to 60 bar are available (e.g., Fig. 10.23, *Endress und Hauser*). The frequency range of these sensors is low, upper cutoff frequencies of approximately 10 Hz are achieved.

The third class is built from foil sensors, distributed, e.g., by the company *Althen GmbH*, Kelkheim, Germany. These capacitive sensor elements are arranged in a matrix with a spacial resolution of $\leq 2 \times 2\,mm^2$. As substrate a flexible polymer foil is used. The height of such an array is 1 mm. The frequency range ranges from static to approx. 1,000 Hz. Nominal loads up to 200 kPa can be acquired with a resolution of 0.07 kPa. Due to creeping (comp. Sect. 10.1.1.3) of the substrate and parasitic capacities, a high measurement inaccuracy exists.

[7] With respect to "force" component.

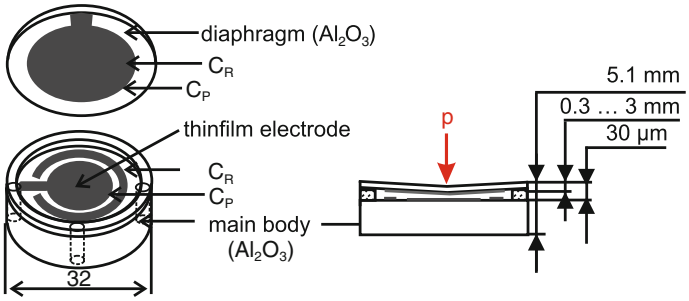

Fig. 10.23 Schematic view of a ceramic pressure sensor fabricated by *Endress und Hauser*, Weil am Rhein, Germany [105]

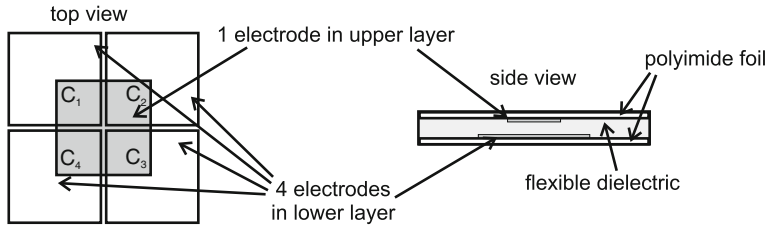

Fig. 10.24 Schematic view of capacitive shear force sensors as presented in [15]

Another polymeric foil sensor in the field of investigation is that one shown in Fig. 10.24 [15]. In contrast to prior examples, this array is used for direct force measurement. Normal forces are detected measuring the change of electrode distance, shear forces by detecting the change of active electrode surface. Similar to the sensors of the company *Althen* static and dynamic changes up to 1,000 Hz can be measured. The spatial resolution is given with $1 \times 1\,\text{mm}^2$. A disadvantage of the design is the high measurement inaccuracy through creeping of the polymer and leakage capacities.

10.1.2.5 Optical Sensors

In the area of optical measurement technology, sensors based on freely propagating beams and fiber optics are available. For force and pressure sensing mainly fiber optic sensors are used, which will be introduced further within this subsection. All fiber optic sensors have in common that mechanical load influences transmission characteristics of the optical transmission network, resulting in an influence of parameters of a reflected or simply transmitted electromagnetic wave. The electromagnetic wave is defined by its wave equation [54].

$$\nabla^2 \Psi = \frac{\delta^2 \Psi}{\delta x^2} + \frac{\delta^2 \Psi}{\delta y^2} + \frac{\delta^2 \Psi}{\delta z^2} \tag{10.24}$$

Ψ represents an arbitrary wave. A possible solution for this differential equation is the propagation of a plane wave in open space. In this case, electrical field E and magnetic field B oscillate orthogonal to each other. Electrical field propagating in z-direction is described by Eq. (10.25).

$$E(z,t) = \frac{1}{2}A(z,t) \cdot e^{j\omega_0 t - \beta_0 z} \tag{10.25}$$

A marks the amplitude of the envelope, ω_0 is the optical carrier frequency, and the propagation constant β_0. With the propagation group velocity $v_g(\lambda)$,[8] the E- and B-field are connected. Depending on the transmitting medium group velocity can be calculated via refraction index n_g [55].

$$v_g(\lambda) = \frac{c_0}{n(\lambda)} \tag{10.26}$$

According to wave length λ, n different values result. Waves are propagating differently depending on their frequency and wavelength. A pulse "spread out". For further information, sources [54, 55, 63, 108] and [56] are recommended. If only mechanical loads such as force or pressure influences the transmission network, the resulting deformation can influence the transmission in two different ways:

1. Material specific: Change of the refraction index n (photoelastic effect)
2. Geometric: Change of beam guidance

The photoelastic effect describes the anisotropy of the refraction index influenced by mechanical stress. Figure 10.25 visualizes this effect. Resulting refraction index change is dependent on applied stress T and is given by the following equation [33]:

$$\Delta n = (n_1 - n_2) = C_0 \cdot (T_1 - T_2) \tag{10.27}$$

C_0 is a material-specific, so-called photoelastic coefficient. T_i marks the resulting internal stress. Depending on refraction index polarization, wave length and phase of beam are changing. In the geometric case, mechanical load changes the conditions of the beam guidance. Using geometrical optics influences of mechanical loads on intensity and phase of radiation can be characterized.

A disturbing source for all fiber optical sensors cannot be neglected: the temperature. Refraction index is depending on temperature changes, and consequently influences the properties of the guided wave. Beside thermal-elastic coefficients describing the strain resulting from temperature changes within any material, temperature directly influences the refraction index itself (Sect. 10.1.2.5). For temperature compensation, a reference fiber has to be used, unloaded, and only influenced by temperature change. An advantage of all fiber optical sensors is given by their immunity to electromagnetic radiation. The following paragraphs introduce the most important principles for optical force and pressure measurement.

[8] In vacuum it is equal to speed of light $c_0 = 2.99792458 \times 10^8$m/s.

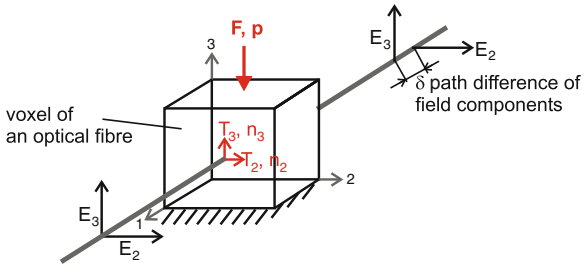

Fig. 10.25 Visualization of photoelastic effect [33]. Due to different refraction indices perpendicularly to the propagation direction propagation velocity of each field component is different and an optical path difference δ occurs. Polarization is changing

Change of Intensity

In principle, two transducer types varying the intensity can be distinguished. Both have in common that mechanical load varies the condition of total reflection (Fig. 10.26). The angle α_c is defined as the critical angle for total reflexion and defined by SNELLIUS' law:

$$\sin(\alpha_c) = \frac{n_2}{n_1} \tag{10.28}$$

The numerical aperture *NA* gives the appropriate critical angle θ_c for coupling radiation into a multimode fiber:

$$\sin(\theta_c) = \sqrt{n_1^2 - n_2^2} \tag{10.29}$$

If the angle varies due to mechanical load and takes values larger than θ_c, respectively, smaller values than α_c, conditions for total reflections are violated. The beam will not be guided within the core of the fiber. Total intensity of the transmitted radiation will become less. Figure 10.27 shows a schematic sketch of the design of the very first variant. The sensor element is attached to the end of a multimode fiber.

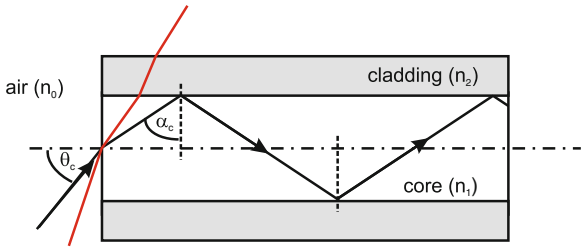

Fig. 10.26 Guidance of multimode fibers. Beams injected with angles above θ_c are not guided in the core

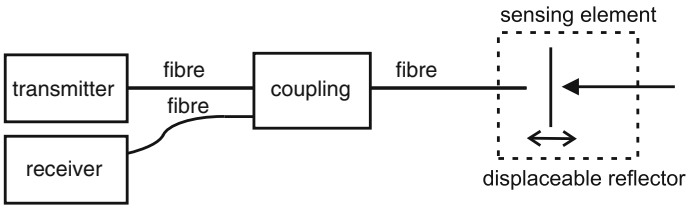

Fig. 10.27 Schematic view of a fiber optic sensor with intensity modulation

In a first variant, the light (e.g., emitted by a laser-diode $\lambda = 1{,}550$ nm) is coupled into a multimode fiber. A reflective element is attached to the end of the transmission line. The element can be designed as a deformable object or a rigid one mounted on a deformable substrate. Mechanical load acts on this object. Due to the load, the reflective element will be deformed (in case of a flexible surface) or displaced (in case of a rigid surface). Varying the displacement, the mode of operation is comparable to a displacement sensor. The intensity is directly proportional to the displacement (Fig. 10.28). The load itself is a function of displacement and directly proportional to the elastic compliance n of the sensor element:

$$F(z) = n \cdot z. \tag{10.30}$$

If the geometry of the area changes, a part of the beam—according to the laws of geometrical optics—is decoupled into the cladding (dispersion) and an intensity loss can be measured at the detector (Fig. 10.28).

In academic publications from PEIRS [67] and KERN [37] such a mode of operation is suggested for multicomponent force measurement. In this case, the measurement

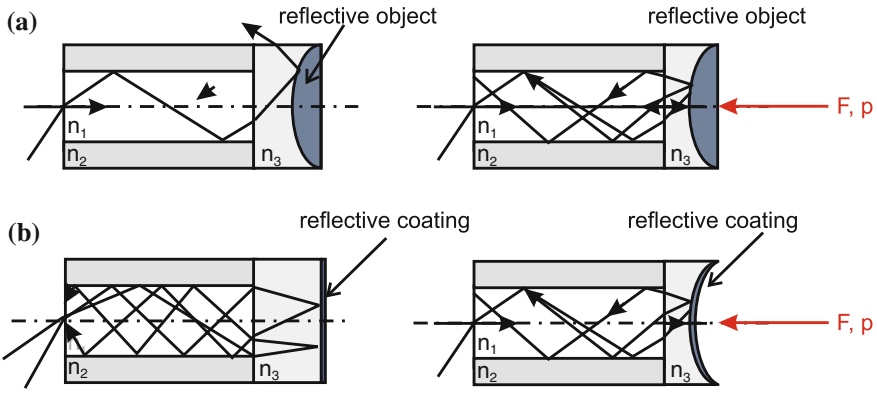

Fig. 10.28 Variation of intensity due to displacement of rigid and flexible elements. **a** Stiff element: intensity is depending on the displacement. **b** Flexible element: intensity is depending on the deformation

range is directly proportional to the mechanical properties of fixation of the reflective body. Using the calculation method known from Sect. 10.1.2.1, this fixation can be designed. A disadvantage of this principal is the use of polymers for the coupling of the reflective object. This leads to creeping of the sensor signal. The measurement inaccuracy of these sensors lies in a range of 10 % [37]. Their diameter takes a value of few millimeters. The length depends on the application. Another source of noise is the temperature. A temperature change leads to a dilatation (or shrinkage) of the polymer itself and displaces the reflective element. The displacement change results in a defective measurement signal. Due to the small size, an array assembly is possible.

The second variant is a so-called microbending sensor. Its fundamental design is schematically given in Fig. 10.29. Like before, a beam is coupled into a multimode fiber. Force, pressure, or strain applied by a comb-like structure results in microbending of the fiber (Fig. 10.29b).

In case of deformation—similar to the first variant—a part of the light is decoupled into the cladding. The intensity of the measured light diminishes.[9] The gaps between the comb-like structures for microbending sensors are in the range of one millimeter. The height of the structure is in the same dimension [92]. To apply mechanical loads, an area of $\cong$1 cm length and a width of $\geq$5 mm is used. Measurement range depends on displacement of the bending structure and diameter of the fiber itself. PANDEY [64] describes the realization of a pressure sensor for loads up to 30 bar. If the bending diameter becomes smaller, lower nominal pressures and forces are possible. Concerning the detection of force components, only one-component sensors can be realized using this principle.

If spatially distributed mechanical load has to be measured, multiple microbending structures can be located along one fiber. To evaluate the several measuring points, for instance optical time domain reflectometry (ODTR) can be used. This device sends a pulsed signal (light pulses of around 10 µs length) guided in a fiber, and measures the reflexion depending on time. Based on the propagation velocity of the

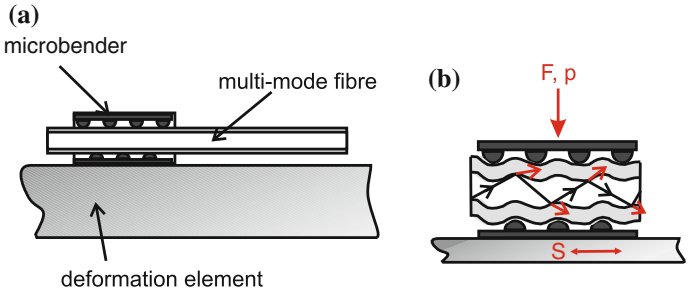

Fig. 10.29 Variation of beam guidance in case of microbending. **a** Assembly of microbending elements. **b** Beam guiding in loading case

[9] Both versions are possible: Measuring the transmitted and the reflected radiation.

beam inside the fiber v, the time delay for each measuring point can be calculated by relating them. Additional information can be found in [48, 92] or [64]. The dynamics of these sensors is only limited by the sensor electronics and could theoretically be applied to the whole range of haptic applications.

Change of Phase

The variation of the phase of light by mechanical load is used for interferometric sensors. The most commonly used type is based on the Fabry-Pérot interferometer, discussed in the following paragraph. Other variants are Michelson- and Mach-Zehnder-interferometers. The assembly is made of two plane-parallel, reflective, and semitransparent objects, e.g., at the end of a fiber, building an optical resonator (Fig. 10.30). The beam is reflected several times within the resonator and interferes with each reflection. The resonance condition of this assembly is given by the distance d of the reflective elements and the refraction index n within the resonator. The so-called free spectral range marks the phase difference δ, generating a constructive superposition of beams:

$$\delta = \frac{2\pi}{\lambda} \cdot 2 \cdot n \cdot d \cdot \cos(\alpha) \tag{10.31}$$

Figure 10.30b shows the typical characteristics of the transmission spectrum of a Fabry-Pérot interferometer. According to the formula shown above the corresponding wavelength yields a transmission peak; all other wavelengths are damped and annihilated. Due to the mechanical load the distance d of the surfaces is varied, changing the conditions for constructive interference. Sensors using this principle are used by the company *LaserComponents Gmbh*, Olching, Germany, for uniaxial

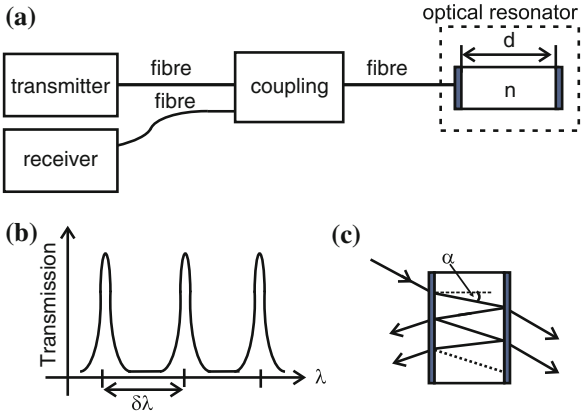

Fig. 10.30 Assembly and operating mode of a Fabry-Pérot interferometer. **a** Schematic assembly of a Fabry-Pérot interferometer. **b** Transmission spectrum. **c** Interferences in a resonator

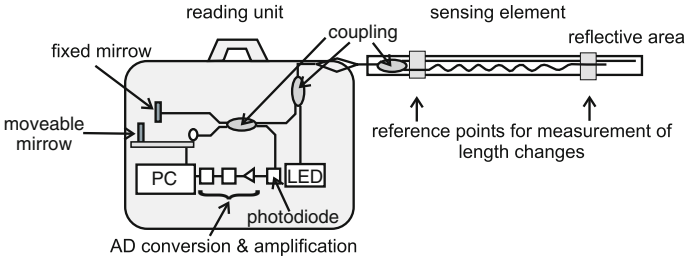

Fig. 10.31 Temperature compensation in interferometric strain-sensing elements [34]

force or pressure measurement, and can be bought for nominal pressures up to 69 bar [45]. The influence of temperature would also appear to be problematic too and has to be compensated by a reference configuration parallel working.

Beside pressure transducers, single-component forces and strains can be measured (Fig. 10.31). The design equals a Michelson-Interferometer. The sensor element is made of two multimode fibers, whereas the strain acts upon only one fiber. Identical to the Fabry-Pérot-configuration, the sensor element is made of two plane-parallel reflective surfaces, whose distance varies according to varying strain. Inside the measuring electronics, a reference design is included. To measure the mechanical load, the phase of reference and measuring assembly is compared. This measurement principle enables to measure frequencies in the range of several kilohertz. The geometrical dimension is given by the diameter of the fiber including some protective coating $\leq$1 mm, and the length of 2–20 mm depending on the application itself. For pressure sensors, the measuring error with respect to nominal load takes a value of about 0.5 %, with strain gages at a factor of 15×10^{-6}.

Change of Wavelength

For optical detection of strain, the so-called fiber BRAGG grating sensors (FBG sensor) are widely used. To realize the sensing element, the refractive index of the core in a single mode fiber is varied due to the position (Fig. 10.32) and a grating arise [83]. The refractive index modulation can be described by

$$n(z) = n_0 + \delta n_{\text{effective}}(z) = n_0 + \delta\overline{n}_{\text{effective}} \cdot \left(1 + s \cdot \cos\left(\frac{2\pi}{\Lambda} z + \phi(z)\right)\right) \quad (10.32)$$

whereas n_0 is the refractive index within the core, $\delta\overline{n}_{\text{effective}}$ is the average of the index's modulation, and s a measure of the intensity of the index's modulation. Λ marks the grating period and the phase shift $\phi(z)$ resulting from the measured value. In idle situation results $\phi(z) = 0$. Figure 10.32 gives a schematic drawing of the assembly.

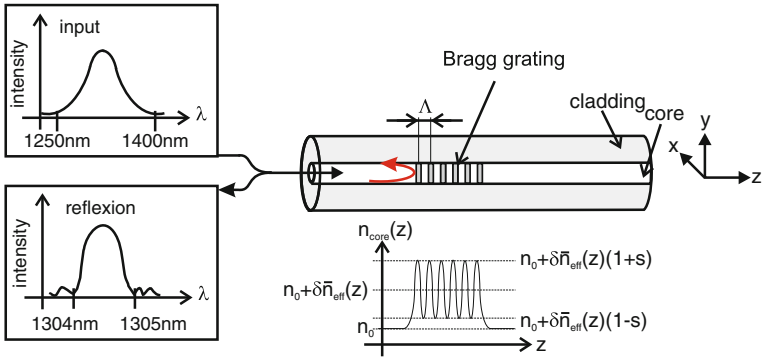

Fig. 10.32 Operational mode of FBG sensors [83]

If light is coupled into the fiber, only parts of it are reflected according to the law of BRAGG. The reflective spectrum shows a peak at the so-called BRAGG-wavelength λ_b. This wavelength depends on the refractive index $n(z)$ and the grating period Λ:

$$\lambda_b = 2n\Lambda. \tag{10.33}$$

In loading case both grating distance and refractive index varies. The maximum of the spectrum is shifting from λ_0 to another wavelength. According to the wavelength shift, mechanical load can be determined. The following condition is achieved:

$$\frac{\Delta\lambda}{\lambda_0} = \underbrace{(1 - C_0)}_{\text{gage factor}} \cdot (S + \alpha_{VK} \cdot \Delta\vartheta) + \frac{\delta n/n}{\delta\vartheta} \cdot \Delta\vartheta, \tag{10.34}$$

whereas α_{VK} is the coefficient of thermal expansion of the deformation body, and C_0 the photoelastic coefficient. Beside the change induced by mechanical strain S, the change of temperature ϑ influences the wavelength shift in the same dimension. Compensating the influence of temperature, another FBG sensor has to be installed as reference at an unloaded area. The temperature compensation is afterward achieved by comparison between both signals. Analogous to resistive strain sensors, a gage factor of $k \approx 0.78$ can be achieved with constant measurement temperature. Extensions up to 10.000 µm/m can be achieved.

The width of the sensor lies in the area of single mode fibers. The sensors length is defined by the grating, which has to be three millimeters at least to provide a usable reflective spectrum [9, 22, 38]. Resolution takes a value of 0.1 µm/m and is—such as its dynamics—defined by the sensor electronics. Similar to strain gages these sensors can be mechanically applied on deformation elements, whose dimensions and shapes define the measurement range. A challenge with the application of fiber sensors in this context is the differing coefficients of thermal expansion between deformable element, adhesive, and fiber. Additionally, reproducibility of

the adhesive-process for fibers is not as high as typically required. Especially creeping of glue results in large measurement errors. Comparable to the microbending principle, FBG sensors are applicable to several spatially distributed measurement points. To distinguish the several positions, gratings with different periods Λ_i and thus different BRAGG-wavelengths λ_b are used. The company *Hottinger Baldwin Messtechnik GmbH*, Darmstadt, Germany, distributes several designs containing an application area around the grid for strain measurement.

Beside monitoring of structures or strain analysis, FBG sensors can be used for realizing force sensors, too. MUELLER describes the use of FBG sensors in a triaxial-force sensor for medical application [59]. Further information on the application of FBG can be found in [9, 22, 83] and [38].

10.1.2.6 Piezoelectric Sensors

Piezoelectric sensors are widely used, especially for measurement of highly dynamic activities. The measurement principle is based on a measure-induced charge displacement within the piezoelectric material, the so-called reciprocal piezoelectric effect (Sect. 9.3). Charge displacement leads to an additional polarization of the material resulting in a change of charge on the materials surface. This can be detected using electrodes (Fig. 10.33). Beside the measurement of force, it is for pressure and acceleration measurement especially. For force measurement, the longitudinal effect is primarily used. Detailed information about the piezoelectric effect and possible designs are found in Sect. 9.3. Materials used for sensing elements will be introduced in the following paragraph.

The general equation of state states for operation in sensor mode:

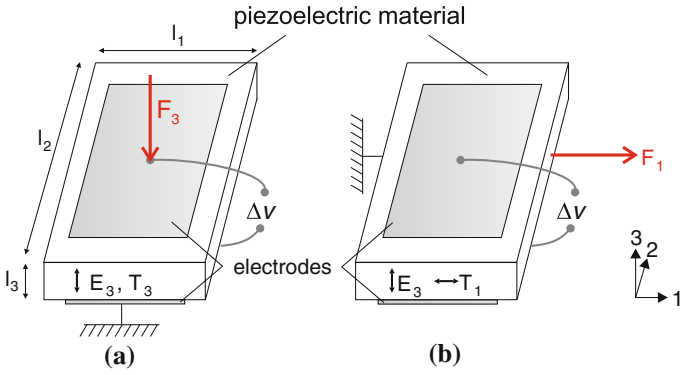

Fig. 10.33 Visualization of piezoelectricity. **a** Longitudinal effect ($E_3 \| T_3$). **b** Transversal effect ($E_3 \| T_1$)

$$D_i = \underbrace{\varepsilon_{ij}^T \cdot E_j}_{\to 0} + d_{im} \cdot T_m, \tag{10.35}$$

$$D_3 = d_{31} \cdot T_1. \tag{10.36}$$

A stress contribution in the sensing material leads to a change of charge density D_i, whereas ε_{ij}^T marks relative permittivity and d_{im} piezoelectric charge constant. Taking geometric parameters of the sensor, electrode area $A = l_1 \cdot l_2$ and thickness l_3 of dielectric, the resulting charge q can be derived. Taking electric parameters into account, sensor output voltage Δu can be calculated [47, 87, 105]:

$$q = D_3 \cdot A_3, \tag{10.37}$$

$$\Delta v = q \cdot \frac{1}{C_\mathrm{p}}, \quad \text{with } C_\mathrm{p} = \frac{e_{33}^T \cdot l_2 \cdot l_1}{l_3}, \tag{10.38}$$

C_p marks capacitance and e_{33}^T piezoelectric force constant.

Technically relevant materials can be distinguished into three groups. The first group is built of monocrystals such as quartz, gallium, and orthophosphate.[10] Polarization change in case of mechanical load is direct proportional to the stress. Its transfer characteristic is very linear and does not have any relevant hysteresis. Piezoelectric coefficients are long-term stable. One disadvantage is the small coupling factor k of about 0.1. For remembrance: k is defined as the quotient transformed to the absorbed energy.

The second group is formed by polycrystalline piezoceramics, such as barium titanate ($BaTiO_3$) or lead zirconate titanate (PZT, $Pb(ZiTi)O_3$), being manufactured in a sintering process. The polarization is artificially generated during the manufacturing process (Sect. 9.3). An advantage of this material is the coupling factor, which is seven times higher than that of quartz. A disadvantage is the nonlinear transfer characteristics with a noticeable hysteresis, and a reduced long-term stability. The materials tend to depolarize.

The last group is build from partial crystalline plastic foils made of polyvinylidene fluoride (PVDF). Its coupling factor lies with 0.1–0.2 in the area of quartz. Advantageous are the limit size (foil thickness of a few µm) and the high elasticity of the material.

The first two sensor materials are used in conventional force sensors, as e.g., distributed by the company *Kistler*. Nominal forces take values of 50 N to 1.2 MN. The sensor typically has a diameter of 16 mm and a height of 8 mm. Alternations of load up to 100 kHz are measurable. Single as well as multiple-component sensors are state-of-the-art. Figure 10.34 shows the general design of a three-component force sensor from *Kistler*.

Piezoelectric force sensors are typically used for the analysis of the dynamic forces occurring during drilling and milling or for stress analysis in automotive industry. In haptic system, these sensor variants can hardly be found. Not exclusively but mostly

[10] This crystal is especially applicable for high temperature requirements.

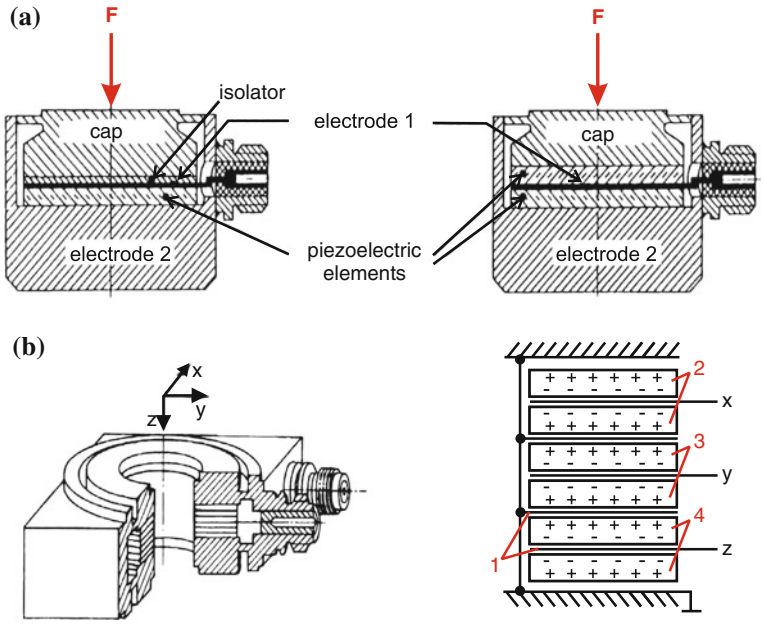

Fig. 10.34 **a** Possible assemblies für piezoelectric force sensors. **b** Assembly of a three-component sensor: *1* electrodes, *2* quartz plates shear effect—F_x, *3* quartz plates longitudinal effect—F_z, and *4* quartz plates shear effect—F_y

because they are not suitable to measure static loads. Sensors based on PVDF-foils as piezoelectric material are increasingly used for the measurement of tactile actions. The piezoelectric effect, however, is used for the generation of a displacement and not for its measurement, making this variant being described in Sect. 10.1.2.7.

10.1.2.7 Less Common Sensing Principles

Sensor designs shown in this subsection are not force or pressure sensors for conventional purposes. All of them have been designed for different research projects in the context of haptic systems. Focus of these developments lies in the spatially distributed measurement of tactile information.

Resonance Sensors

For measurement of vibrotactile information, e.g., the so-called resonance principle could be used. Figure 10.35a shows the principal design of such a sensor. A piezoelectric foil (PZT or even PVDF) is used as an actuator. Electrodes on both sides of the foil apply an electrical oscillating signal, resulting in mechanical oscillations

of the material due to the direct piezoelectric effect. The structure oscillates at its resonance frequency f_0 calculated by the following formula

$$f_0 = \frac{1}{2d} \cdot \sqrt{\frac{n}{\rho}} \tag{10.39}$$

whereas d is the thickness, n the elasticity, and ρ the density of the used material. The load, responsible for the deformation, is proportional to the frequency change [70]. For spatially distributed measurement, the sensors are connected as arrays of elements with 3×3 and 15×15 sensors. The dimensions of the sensing arrays takes values of 8×8 mm^2, respectively, 14×14 mm^2. The thickness of the foil is $\ll$1 mm. A huge disadvantage of this principle is the high temperature dependency of the resonance frequency from the piezoelectric material used. The coefficient lies at 11.5 Hz per 1 °C within a temperature range between 20 and 30 °C [26, 41].

The so-called surface acoustic wave resonators, SAW sensors, make use of the change of their resonance frequency too. The excitation occurs via an emitter called "Inter-digital structure" (Fig. 10.35b). The mechanical oscillations with frequencies in the range of MHz distribute along the surface of the material. They are reflected on parallel metal structures and detected by the receiving structure. Due to mechanical values applied the material is deformed, the runtime of the mechanical wave changes, and consequently the sensor's resonance frequency. With this design, the temperature is one of the major disturbing values. SAW sensors are used for measurement of force, torques, pressure, and strain. The dynamic range reaches from static to highly dynamic loads.

Electrodynamic Sensor Systems

Within the research project *TAMIC* an active sensor system for the analysis of organic tissue in minimally invasive surgery was developed [29]. The underlying principle is

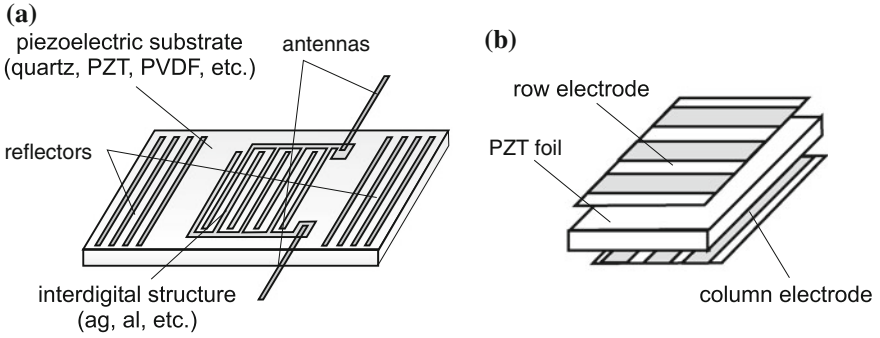

Fig. 10.35 Schematic view of resonance sensors. **a** Principle of a surface acoustic wave resonator [72]. **b** Principle of a resonant sensor array [70]

based on an electrodynamic actuated plunger excited to oscillations (see Sect. 9.1). The plunger is magnetized in axial direction. The movements of the plunger induce voltages within an additional coil included in the system. The material to be measured is damping the movement, which can be detected and quantified by the induced voltage. The maximum displacement of the plunger is set to one millimeter. The system is able to measure dynamically from 10 to 60 Hz. The nominal force lies in the range of 200 mN. The geometrical dimensions of the system are a diameter of $\leq$15 mm, and a length of $\leq$400 mm, which is near to typical minimally invasive instruments. Detailed information can be found in [84].

Another example for a miniaturized sensor for the measurement of spatially distributed tactile information is presented by HASEGAWA in [30]. Figure 10.36 shows the schematic design of one element.

The elements are arranged in an array structure. In quasi-static operation mode the system is able to measure contact force and the measurement object's elasticity. The upper surface is made of a silicon-diaphragm with a small cubical for force-application to the center of the plane. The displacement of the plate is measured identical to a silicon-pressure or -force sensor with piezoresistive areas on the substrate. By the displacement, the applied contact force can be derived. For measuring the elastic compliance of the object, a current is applied to the flat coil (Fig. 10.36). In the center of the diaphragm's lower side a permanent magnet is mounted. The electrically generated magnetic field is oriented in the opposite direction of the permanent magnet. The plate is displaced by this electromagnetic actuator and the cube is pressed back into the object. The force necessary to deform the object is used in combination with the piezoresistive sensors signal for calculation of the object's elastic compliance. In the dynamic operation mode, the coil is supplied with an oscillating signal, operating the diaphragm in resonance. Due to interaction with the measured object, the resonance condition changes. By the changing parameters, such as phase rotation, resonance frequency, and amplitude, elastic coefficients such as damping coefficients of the material can be identified. Due to the high degree of miniaturization, highly dynamic actions up to several kilohertz are possible to be

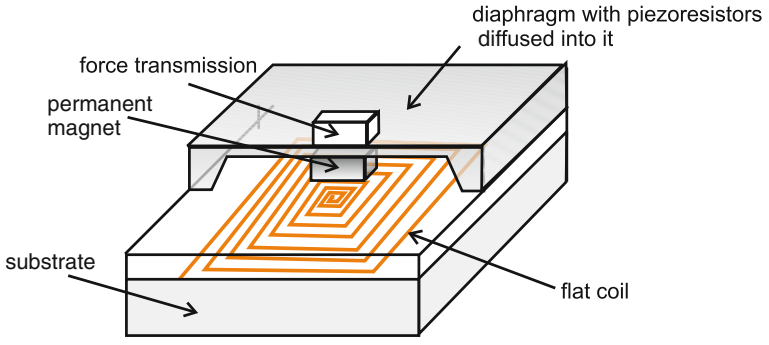

Fig. 10.36 Schematic view of an active element [30]. The dimensions are $6 \times 6 \times 1$ mm^3

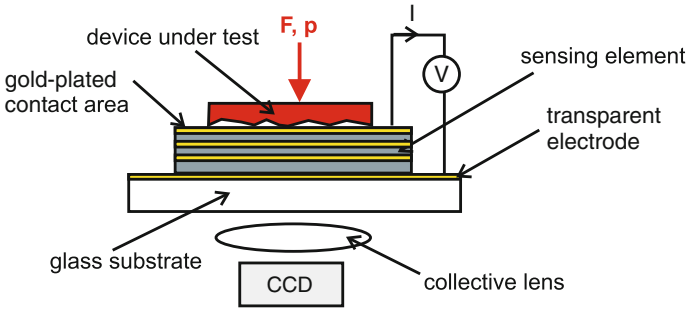

Fig. 10.37 Schematic view of an electroluminiscence sensor [79]

measured. The nominal force lies in the area of 2 N, the resolution of the system is unknown.

Electroluminescence Sensors

A high-resolution touch sensor is presented by SARAF [79]. It is thought to be used for the analysis of texture on organ surfaces. Figure 10.37 shows a schematic sketch. On a transparent glass substrate, a layer-compound of 10 µm height made of gold- and cadmium sulfite particles[11] is applied. The single layers are separated by dielectric barriers. The mechanical load is applied on the upper gold layer, resulting in a breakthrough of the dielectric layer and a current flow. Additionally, energy is released in form of small flashes. This optical signal is detected using a CCD-camera. The signal is directly proportional to the strain distribution generated by the load. The resulting current density is measured and interpreted.

The spatial resolution of the design is given with 50 µm. Nominal pressures of around 0.8 bar can be detected. The sensor area has a size of 2.5×2.5 mm^2, the thickness of the sensor is $\leq$1 mm and thus very thin. Additional information can be found in [79].

10.1.3 Selection of a Suitable Sensor

In earlier sections, sources for the requirements identification have been presented. Afterward, presentation and discussion of the most relevant sensor principles to measure forces were made. This section is intended to help engineers to select or even develop an appropriate force sensor. Depending on the identified requirements found using Sect. 10.1.1, a suitable sensor principle can be chosen.

[11] A semiconducting material.

Table 10.4 Compilation of main requirements on haptic sensors

Type of information	Requirements	Values
Kinaesthetic	Nominal load F_N	(5–100) N
	Resolution ΔF	5 % F_N
	Frequency range	(0–10) Hz
Tactile	Nominal load F_N	$\leq$0.3 N or $\leq$4.5 N
	Resolution ΔF	5 % F_N
	Frequency range	(0–1,000) Hz
	Spatial resolution Δx	Structural dependent, $\geq$0.5 mm

Depending on system topology and measurement task further requirements have to be considered

To get a better overview, the basic requirements described in Sect. 10.1.1.5 are collected in Table 10.4. The requirements are distinguished concerning human perception in kinaesthetic and tactile information. More detailed information concerning force and spatial resolution can of course be found in Sect. 10.1.1. The properties of active and passive transformers—force measurement is done via a mechanical variable such as strain or stress detected via elastomechanics—are strongly dependent on the design of the deformation element. Especially the nominal force, number of components to be measured, and the dynamics are directly influenced by the deformation element's design.

A comparison of all sensor principles can hardly be done. Consequently, the methods will be compared separately from each other. As evaluation criteria, transfer characteristics and geometrical dimensions are chosen. Figure 10.38 classifies the principles according to gage factor and geometry. According to the increasing size of the strain-sensing element, the whole-force sensor can be designed at a higher level

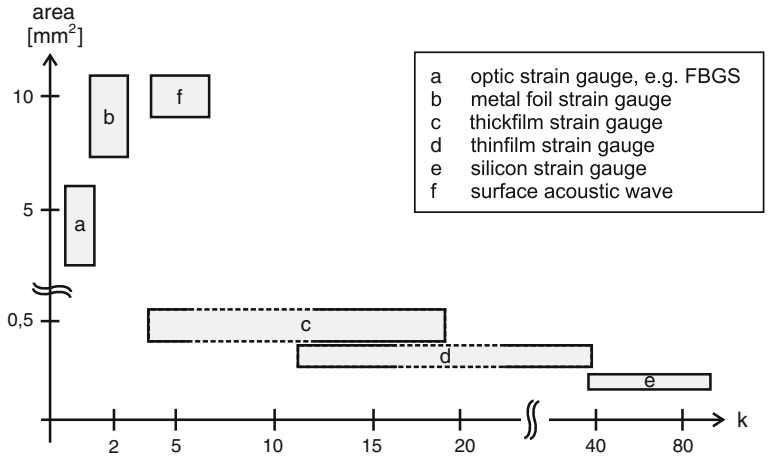

Fig. 10.38 Comparison of different strain measurement technologies due to dimensions and gage factor

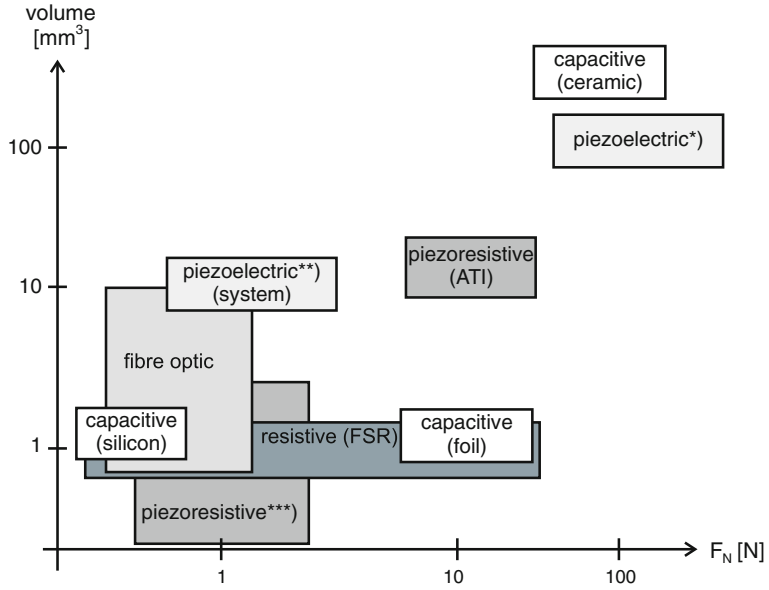

Fig. 10.39 Comparison of different measurement technologies due to dimensions and nominal load. ∗ Commercial force/torque sensors. ∗∗ Active sensor systems classified as exotic sensors. ∗∗∗ Tactologic system

of miniaturization. A direct result of smaller size is the minimized mass, providing an increased upper cutoff frequency. If the gage factor of the sensing element is higher, lower absolute value of strain is necessary to get a high output signal. Additionally, the overall design can be designed stiffer. This enables to detect smaller nominal forces and thus higher cutoff frequencies. Concerning the lower cutoff frequency, strain-sensing elements are suitable for measuring static loads. Using piezoresistive and capacitive silicon sensors, an upper cutoff frequency of 10 kHz or more can be measured with high resolution.

The other sensor principles can be compared contingent on nominal load and dimensions. Figure 10.39 classifies the presented principals according to their nominal load and corresponding construction space.

Except the piezoelectric sensors, all sensor principles can be used for measuring static and dynamic loads. The upper cutoff frequency mainly depends on the mass of the sensor which has to be moved. Consequently, the more miniaturized the sensor, the higher the upper cutoff frequency becomes. Figure 10.40 compares the presented sensor principles according to the detectable nominal load and the corresponding dynamic range.

By means of the shown diagrams a preselection of suitable sensor principles for the intended application can be done. Additional sensor properties such as resolution, energy consumption, costs, or impact of noise are strongly depending on the individual realization and will not be taken into account here. Advanced descriptions of

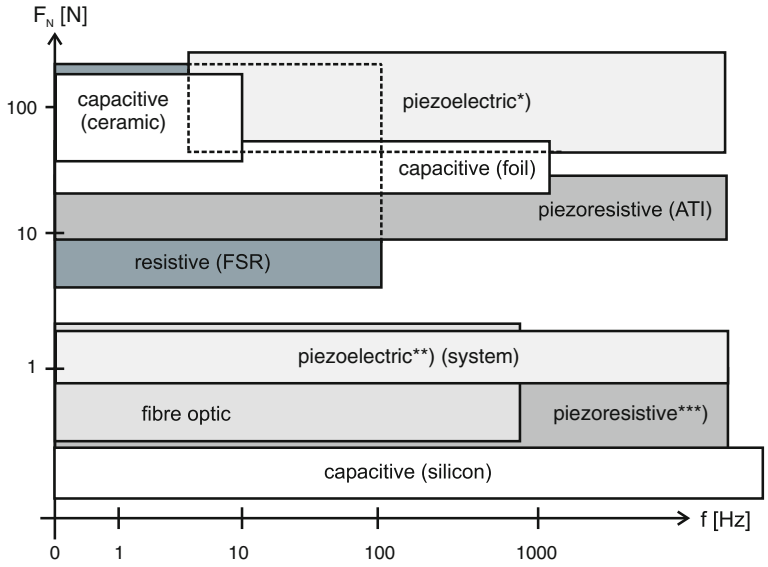

Fig. 10.40 Comparison of different measurement technologies due to nominal load and frequency range. ∗ Commercial force/torque sensors. ∗∗ Active sensor systems classified as exotic sensors. ∗∗∗ Tactologic system

sensor properties have to be taken from the literature highlighted in the corresponding subsections for the individual principle.

To give an example of how to select a suitable force sensor, the task *laparoscopic palpation of tissue* is chosen. Figure 10.41 shows the tree diagram which can be used for analyzing the task and deriving requirements. Laparoscopic palpation is a telemanipulation task for characterizing texture. It is done via closed-loop control. To avoid undesired influences of the laparoscopic instrument itself onto the sensing signal (e.g., friction between instrument and abdominal wall), the sensor should be integrated into the tip. The laparoscope is used to scan the tissues surface. Detecting three directions of contact force, texture and even compliance of tissue can be analyzed.

Taking contact information into account (see Table 10.4) cutoff frequency, resolution, and nominal force can be derived. The dimensions of the laparoscope limit the construction space. Also static information has to be measured, thus an active sensing principle-like (piezo-)resistive, capacitive, inductive, or optic should be considered. Due to limited space, piezoresistive sensing is recommendable.

If no force sensor with the determined requirements is available, a deformation element has to be designed separately taking load condition and elastomechanics into account. For example, [11, 72] are helpful references for designing deformation elements. The strain-sensing element can be chosen depending on the aimed resolution and construction space. Table 10.5 gives an overview of common strain-sensing technologies.

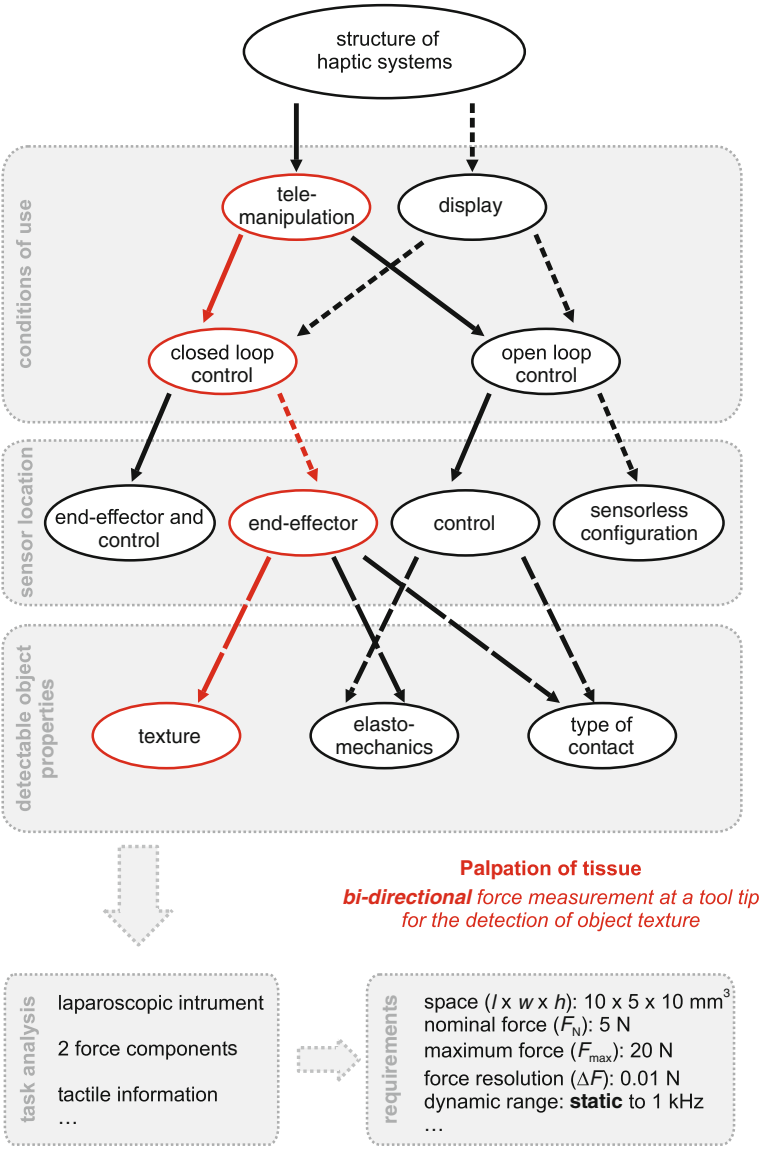

Fig. 10.41 Tree diagram for selecting a force sensor. Exemplarily, the task *laparoscopic palpation of tissue* is chosen

Table 10.5 Comparison of common sensing principles for strain measurement [72]

Principle	Material	Gage factor	S_{min}	S_N (%)	S_{max} (%)	Thickness h_M (µm)	References
Foil-strain gage	Constantan	2.0	$\pm 10^{-7}$	±0.1	±2	80–100	[32, 35, 91]
Thick-film	$Bi_2Ru_2O_7$	12.1–18.3	$\pm 10^{-6}$	±0.1	±0.2	≤50	[3, 65]
	PEDOT:PSS	0.48–17.8	–	≥10[a]	–	1–10	[44, 46]
Thin-film[b]	TiON	4–5	$\pm 10^{-7}$	±0.1	±2	≤1	[3, 42, 105]
	Poly-Si	20–30	$\pm 10^{-7}$	±0,1	±2	≤1	[3, 105]
Si-Technology	Homogeneous	100–255	$\pm 10^{-6}$	±0.2	±0.3	10–15	[58]
	Inhomogeneous	80–255	$\pm 10^{-7}$	±0.05	±0.1[c]	17–100	[5, 23]
Capacitive	PVDF[d]	≤83	–	±0.3	±1	About 150	[2]
	Inter-digital	1–5	$\pm 10^{-7}$	±0.1	±5	≤500	[3, 50, 94]
FBGS	–	0.78	$\pm 10^{-7}$	±0.2	±1	150–250	[77, 82]
Piezoelectric	PZT[e]	$\leq 2 \times 10^6$	$\pm 10^{-10}$	–	±0.1	200	[25, 69]
SAW	Quartz	1.28–20	$\pm 10^{-7}$	±1	±2	About 600	[57, 74, 97, 105, 109]
Magneto-elastic	NiFe45/55	About 1,500	$\pm 10^{-8}$	±0.2	–	About ≤80 µm	[1, 47, 66]
Fibers	Carbon	1.3–31	–	–	0.2–15	12	[16, 43]

[a] Depending on substrate, in [14] polymeric fibers with a maximum strain of 10 % are used
[b] Maximum strain depends on elasticity of deformation element
[c] According to [51] elongation of break takes a value of ±0.2 %
[d] $d\varepsilon/\varepsilon$, sandwich-topology
[e] Patch transducer, PI

10.2 Positioning Sensors

Thorsten A. Kern

To acquire the user's reaction in haptic systems, a measurement of positions, respectively and their time derivatives (velocities and accelerations) is necessary. Several measurement principles are available to achieve this. A mechanical influence of the sensor on the system has to be avoided for haptic applications, especially kinaesthetic ones. Consequently, this discussion focuses on principles which do not affect the mechanical properties significantly. Beside the common optical measurement principles, the use of inductive or capacitive sensors is promising especially in combination with actuator design. This chapter gives an overview about the most frequently used principles, amended by hints for their advantages and disadvantages when applied to haptic systems.

10.2.1 Basic Principles of Position Measurement

For position measurement, two principle approaches can be distinguished: differential and absolute measuring systems.

10.2.1.1 Incremental Principle

Differential systems acquire the change in discrete steps together with the direction of change, and protocol (typically: count) these events. This protocol has to be set back to a reference position by an external signal. If no step loss happens during movement, a prior initialized differential system is able to provide the absolute position as output. If this initializing reference position is set in point which is passed often, a differential system will be referenced frequently during normal operation. Potential step losses would then affect the time till the next initializing event only.

Measurement of the steps is done via a discrete periodic event, typically encoded in a code disc with grooves or a magnetic rotor. This event is transformed by the sensor in a digital signal, whose frequency is proportional to the velocity of the movement (Fig. 10.42a). Some additional directional information is required to be able to measure the absolute position. A typical solution for this purpose is the use of two identical event types with a phase shift (between 1 and 179°, typically 90°. By looking at the status (*high/low*) of these incremental signals (Fig. 10.42b) at, e.g., the rising edges of the first incremental signal (A), a *low* encodes one movement direction, and a *high* encodes the opposite movement direction. Accordingly, the count process either adds or subtracts the pulses generated—in this case—by the second signal (B). State-of-the-art microcontrollers are equipped with counters for incremental measurement already. They provide input pins for count-signal and count-direction. Discrete counters are sold as "Quadrature-Encoder" ICs and

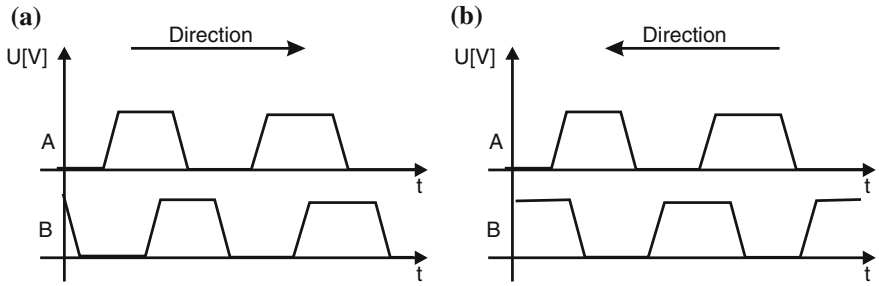

Fig. 10.42 Principle of direction detection with two digital signals with a 90° phase-lag

frequently include actuator drive electronics, which can be applied for positioning tasks. Latter prevents them from being useful for typical haptic applications.

10.2.1.2 Absolute Measurement Principle

Absolute measurement systems acquire a position- or angle-proportional value directly. They are usually analog. A reference position for these systems is not necessary. They have advantages with reference to their measurement frequency, as they are not required to measure with dynamics defined by the maximum movement velocity. The acquisition dynamics of incremental principles is given by the necessity not to miss any events. In case of absolute measurement principles, the measurement frequency can be adjusted to the process-dynamics afterward, which is usually less demanding. However by the analog measurement technology the efforts are quite high for the circuit, the compensation of disturbances, and the almost obligate digitization of the analog signal.

An alternative for the pure absolute measurement with analog technology is given by a discrete absolute measurement of defined states. In Sect. 9.2.2.1, Fig. 9.15, a commutation of EC-drives with a discrete, position coding of magnet-angles with field plates was already shown. This approach is based on the assumption to achieve a discrete resolution of ΔD from m measurement points with n states by

$$n^m = \Delta D. \tag{10.40}$$

In case of the commutated EC-drive $m = 3$ measurement points, which are able to have $n = 2$ states, could encode eight positions on the circumference, but only six were actually used. But there are other more complex code discs with several lanes for one sensor each. These sensors are usually able to code two states. However, e.g., by the use of different colors on the disc many more states would be imaginable. A resolution of, e.g., 1degree (360 discrete steps) would need the number of

$$m = \frac{\log(\Delta D)}{\log(n)} = 8.49 \tag{10.41}$$

at least nine lanes for encoding.

10.2.2 Requirements in the Context of Haptics

Position measurement systems are primarily characterized by their achievable resolution and dynamics. For haptic devices, in dependence on the measurement basis for computer mice and scanners, position resolutions are frequently defined as dots-per-inch ΔR_{inch}. Consequently, the resolution ΔR_{mm} in metric millimeters is given as:

$$\Delta R_{\text{mm}} = \frac{25,4\,\text{mm} \times \text{dpi}}{\Delta R_{\text{inch}}}. \tag{10.42}$$

A system with 300 dpi resolution achieves an actual resolution of 84 µm. In dependency on the measurement principle used, different actions have to be taken to achieve this measurement quality. With incremental measurement systems, the sensors for the acquisition of single steps (e.g., holes on a mask) are frequently less resolutive, requiring a transformation of the user's movement to larger displacements at the sensor. This is typically achieved by larger diameters of code discs and measurement at their edge. These discs are mounted on an axis, e.g., of an actuator. With analog absolute systems, an option for improving the signal is conditioning. It is aimed at reducing the noise component in the signal relative to the wanted signal. This is usually done by a suppression of the noise source (e.g., ambient light), the modulation, and filtering of the signal (e.g., lock-in amplifier, compare Sect. 10.2.6) or the improvement of secondary electronics of the sensors (high-resolution A/D-transformer, constant reference sources).

Beside the position measurement itself, its dynamic has to be considered during the design process. This requirement is relevant for incremental measurement systems only. Absolute measurement systems need a bandwidth equal to the bandwidth provided by the interface and the transmission chain (Chap. 11) for positioning information. Incremental measurement systems, however, have to be capable of detecting any movement event, independent from the actual movement velocity. The protocol format, usually given by counters part of the microcontrollers, has to be dimensioned to cover the maximum incremental frequency. This requires some assumptions for the maximum movement velocity v_{max}. If a system with 300 dpi position resolution moves at a maximum velocity of 100 mm/s, the dynamic f_{ink} for detecting the increments is given as

$$\frac{1}{f_{\text{ink}}} = \frac{\Delta R_{\text{mm}}}{v_{\text{max}}} \tag{10.43}$$

For the example, the necessary measurement frequency is given with $f_{\text{ink}} = 1{,}190\,\text{Hz}$. The effective counting frequency is usually chosen with factor two to four higher than that to have a security margin for counting errors and direction detection.

10.2.3 Optical Sensors

Optical sensors for position measuring are gladly and frequently used. They excel by their mechanical robustness and good signal-to-noise ratios. They are cheap and in case of direct position measurement quite simple to read out.[12]

Code Discs

Code discs represent the most frequently used type of position measurement systems with haptic devices, especially within the class of low-cost devices. They are based on transmission (Fig. 10.43a) or reflection of an optical radiation, which is interrupted in discrete events. The necessary baffle is located near to the receiver. It is manufactured by stamping, or printed on a transparent substrate (glass, plastic material) via thick-film technology or laser printers. For high requirements on resolution, they are made of metal, either self-supportive or on a substrate again. In these cases, the openings are generated by a photolithographic etching process. The receivers can be realized in different designs. Figure 10.43 shows a discrete design with two senders in form of diodes and two receivers (photodiode, phototransistor). The placement of sender/receiver units have to allow the phase shift for directional detection (see Sect. 10.2.1.1). An alternative is given by fork light barriers already including a compact sender/receiver unit. Additionally opto-encoders (e.g., HLC2705) exist including the signal conditioning for direction detection from the two incremental signals. The output pins of these elements provide a frequency and one signal for the direction information.

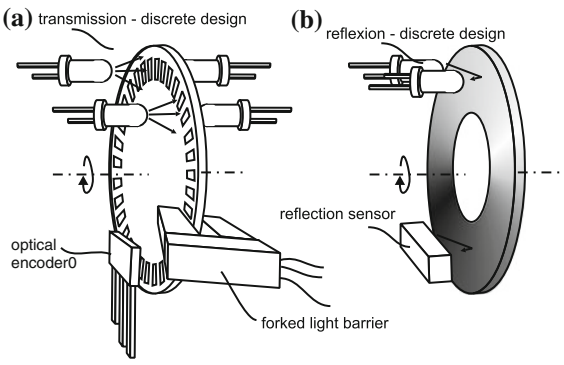

Fig. 10.43 Incremental optical position measurement (**a**), and absolute position measurement via grayscale values (**b**)

[12] The examples presented here are discussed either for translatory and rotatory applications. But all principles may be applied to both, as a translation is just a rotation on a circle with infinite diameter.

Gray Scale Values

With similar components, but for absolute measurement a grayscale disc or grayscale sensor can be built. Once again there are transmission and reflection (Fig. 10.43b) variants of this sensor. In any case the reflection/transmission of the radiation varies depending on the angle or position of a code disc. The amplitude of the reflection gives absolute position information of the disc. For measurement, once again, either a discrete design or the usage of integrated circuits in the form of the so-called reflection sensors is possible. Although such sensors are frequently used as pure distance switches only, they show very interesting proportional characteristics between the received numbers of photons and their output signal. They are composed of a light emitting diode as sender and a phototransistor as receiver. In some limits, the output is typically given by a linear proportional photoelectric current.

Reflection Light Switches

Reflection light switches show useful characteristics for a direct position measurement too. In the range of several millimeters, they have a piecewise linear dependency between photocurrent and the distance from the sensor to the reflecting surface. Consequently, they are useful as sensors for absolute position measurement of translatory movements (Fig. 10.44a). By this method, e.g., with the SFH900 or its SMD successor SFH3201 within a near field up to $\approx$1 mm measurement inaccuracies of some micrometers can be achieved. In a more distant field up to 5 mm, the sensor is suitable for measurement inaccuracies of $\frac{1}{10}$ mm still.

Mice-Sensor

The invention of optical mice without ball resulted in a new sensor type interesting for other applications too. The optical mice sensors are based on an IC measuring an illuminated surface through an optic element (Fig. 10.44b). The resolution of the CMOS sensors typically used range from 16 $\times$ 16 to 32 $\times$ 32 pixels. By the image

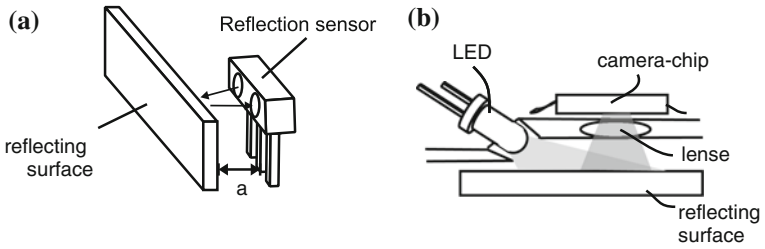

Fig. 10.44 Distance measurement with reflection light switches (**a**), and via the movement of an reflective surface in two DoFs "mouse-sensor" (**b**)

acquired the chip identifies the movement of contrast difference in their direction and velocity. The interface of the calculated values varies from sensor to sensor. The very early types provided an incremental signal for movements in X- and Y-direction identical to approaches with code discs described above. They additionally had a serial protocol included to read the complete pixel information. Modern sensors (e.g., ADNB-3532) provide serial protocols for a direct communication with a microcontroller only. This allowed a further miniaturization of the IC and a minimization of the number of contact pins necessary. The resolution of state-of-the-art sensor is in between 500 and 1000 dpi and is usually sufficient for haptic applications. Only the velocity of position output varies a lot with the sensor types available at the market, and has to be considered carefully for the individual device design. The frequency is usually below 50 Hz. Additionally, early sensor designs had some problems with drift and made counting errors, which could be compensated only by frequent referencing.

The sensors are usually sold for computer-mouse-similar applications and corresponding optics. Besides that it is also possible to make measurements of moving surfaces with an adapted optic design at a distance of several centimeters.

Triangulation

Optical triangulation is an additional principle for contactless distance measurement; however, it is seldom used for haptic devices. A radiation source, usually a laser, illuminates the surface to be measured, and the reflected radiation is directed on different positions along a sensor array (Fig. 10.45). The sensor array may be made of discrete photodiodes. Frequently, it is a CCD or CMOS row with the corresponding

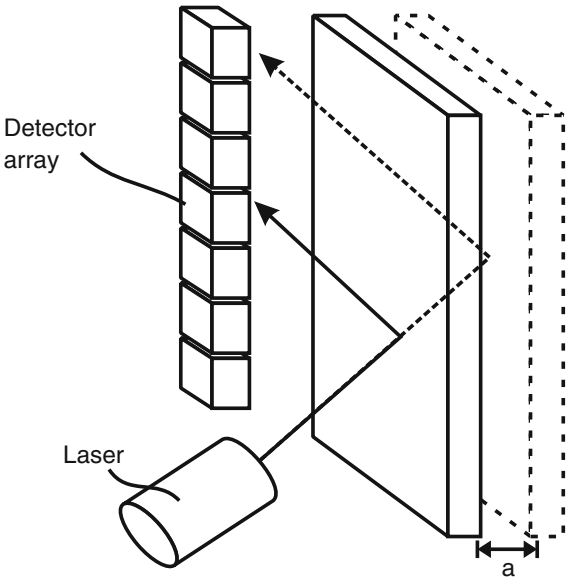

Fig. 10.45 Triangulation of a distance with laser-diode and detector array

high resolution. By focal point identification weighting of several detectors, a further reduction of measurement inaccuracy can be achieved. Compared to other optical sensors, triangulation sensors are expensive as the detection row with a sufficient resolution is a high-cost factor. Their border frequency ($\gg$1 kHz) and their measurement inaccuracy ($<$10 μm) leave nothing to be desired. It is one of the very few principles which can hardly be used for measuring rotating systems.

10.2.4 Magnetic Sensors

Beside the optical measurement principles, especially the group of magnetic measurement principles is relevant for haptic devices. This is a consequence from the fact that electrodynamic and electromagnetic actuators already require magnetic fields to generate forces. For systematization, sensors for static fields, field plates, and hall-sensors, and sensors for induced currents and time-dependent fields can be distinguished.

Field Plates or Magnetic-Dependent Resistors

Field plates or magnetic-dependent resistors (MDR) are two pole elements with the resistance being controlled by the presence of a magnetic field. They make use of the GAUSS effect, which is based on charge carriers being displaced by the LORENTZ force when crossing a magnetic field. The resulting increase of the path length [61] requires an increase of the ohmic resistance of the material. The parameter characterizing this dependency is dependent on the electron mobility and the path length in the magnetic field. A frequently used material is InSb with very high electron mobility. For an additional increase of the effect, the conductor is formed like in the shape of a meander similar to strain gages. MDRs are not sensitive to the polarity of the magnetic field. They are detecting the absolute value only. The increase of resistance is nonlinear and similar to a characteristic curve of a diode or transistor. A magnetic bias is recommended when using the plates to make sure they are in their linear working point.

Hall-Sensors

Hall-sensors are based on the GAUSS effect too. In contrast to field plates, they are not measuring the resistance increase of the current within the semiconductor, but the voltage orthogonal to the current. This voltage is a direct result of the displacement of the electrodes along the path within the material. The resulting signal is linear and bipolar in dependency on the field-direction. ICs with an integrated amplifier electronics and digital or analog output signals can be bought off the shelf. A frequent use can be found with sensors being located at a phase angle α with diametral magnetized rotational magnets (Fig. 10.46). In this application, rotation and rotation-direction are measured.

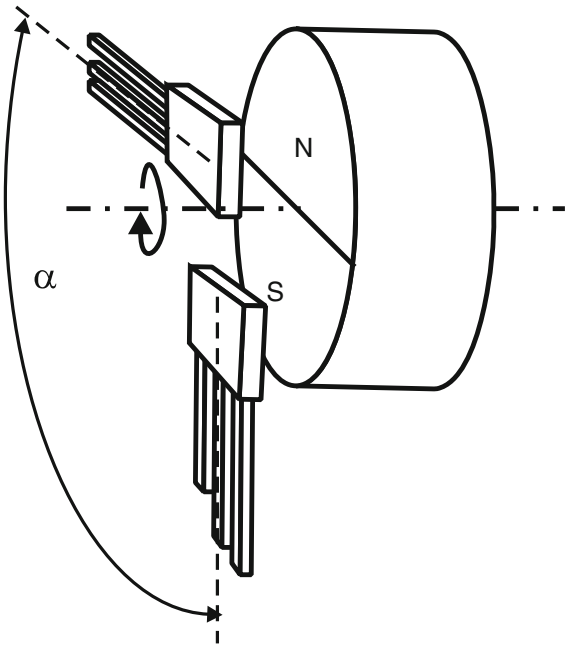

Fig. 10.46 Measurement of the rotation angle of a magnet via field plates or hall-sensors

Inductance Systems

An often forgotten alternative for position measurement is the measurement of changing inductances. The inductance of a system is dependent on many parameters, for example, the magnetic permeability of a material in a coil. Using a differential measurement in between two coils (Fig. 10.47b), a displacement measurement can be made, if a ferromagnetic material moves in between both coils as a position-depending core. As alternatives, the geometry of the magnetic circuit may be changed or its saturation may influence the inductance of the coils. Latter approach is used in systems, where grooves on a ferromagnetic material trigger events in a nearby coil (Fig. 10.47a).

A simple electronic method for measuring inductance is the use of a LR-serial circuit, which—for example with a microcontroller—is triggered with a voltage step. The measurement value is given by the time the voltage at the resistor needs to trigger a comparator voltage. The duration encodes the inductance, assuming a constant resistance. For the actual design, it has to be considered that the winded coil has an own resistance which cannot be neglected. As an alternative a frequency nearby the resonance $\frac{L}{R}$ of the LR-circuit can be applied. The voltage amplitude measured varies dependent on the inductance detuned by the movement of the ferromagnetic core.

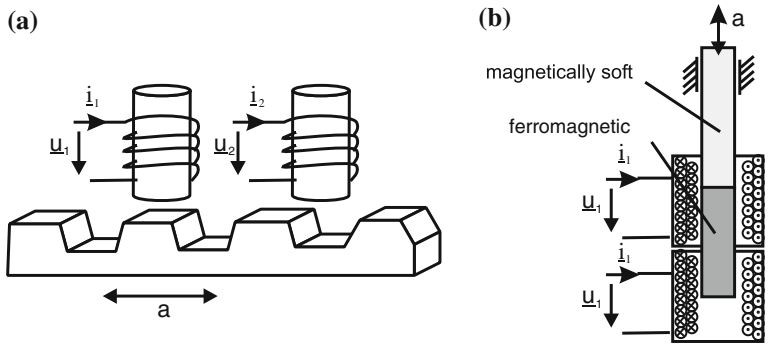

Fig. 10.47 Incremental measurement of a movement via induced currents (**a**) and differential measurement of the position of a ferromagnetic core (**b**)

10.2.5 Other Displacement Sensors

Beside the displacement measurement principles discussed above, there are some rarely used principles still worth to be mentioned here.

Ultrasonic Sensors

Ultrasonic sensors (Fig. 10.48) are based on the running time measurement in between the emission of acoustic oscillations and the moment of the acquisition of their reflection. The frequency chosen is dependent on the requirements on measurement accuracy and the medium for propagation of the wave. As a rough rule of thumb, the denser a material is, the less the damping becomes for acoustic waves. For measurement in tissue frequencies between 1 and 40 MHz are applied. In water frequencies between 100 and 500 kHz and in the atmosphere frequencies well below 30 kHz are used.

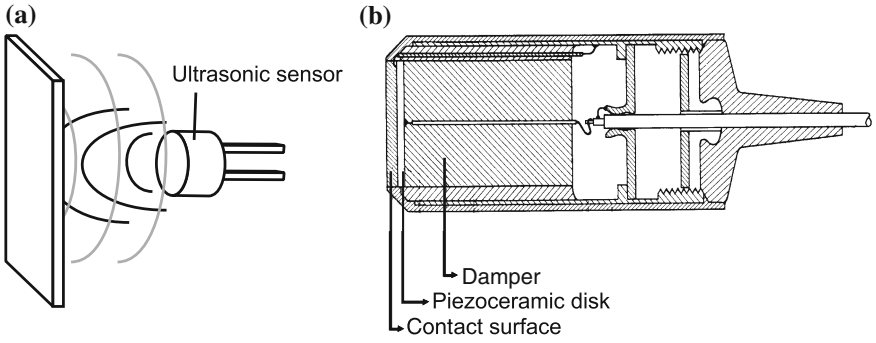

Fig. 10.48 Distance measurement via ultrasonic sensors (**a**) and cross section through a medical ultrasonic head with fixed focus (**b**)

Whereas with medical applications in tissues the medium shows a damping quite linear in the range of 1 dB/Mhz/cm, the measurement within the atmosphere is strongly dependent on the frequency chosen and usually nonlinear. Additionally, the acoustic velocity is dependent on the acoustic density of the medium. For the transversal direction—typically used for measurement—velocities between 340 m/s for air and 1,500 m/s for water can be achieved. According to the wave theory, the minimum measurement accuracy possible in transversal direction is $\frac{\lambda}{2}$, which is coupled to both factors mentioned above. It is a natural border of minimum resolution to be achieved.

The most frequently used source and receiver for the mechanical oscillation are piezoelectric materials (Fig. 10.48b), whose step response oscillations are sharpened by a coupled mass.

Capacitive Sensors

In Sect. 9.5, the equations for the calculation of capacities between plates of electrostatic actuators (Eq. 9.75) were introduced. Of course the measurement of a variable capacity, especially with the linear effect of a transversal plate displacement, can be used for position measurement. This is especially interesting if there are conductive components in the mechanical design, which already move relative to each other. As the capacity is very much dependent on the permittivity of the medium between the plates, which can be strongly influenced by oil or humidity, such a measurement can be done on insusceptible or other well-housed actuators only. Additionally, leakage fields of conductors or geometries nearby are usually of the same size as the capacity to be measured. But capacitive sensors for haptic devices can be found in the context of another interesting application. The measurement of the capacity of the handle, even when isolated by a nonconductive layer, allows identifying a human touch very securely.

10.2.6 Electronics for Absolute Positions Sensors

The absolute measurement of a position requires, as mentioned earlier, some additional effort in the electronic design compared to discrete sensors. Two aspects shall be discussed in the context of this chapter.

Constant Current Supply and Voltage References

For the generation of a constant radiation or the measurement of a bridge circuit, the use of constant currents is necessary. There is always the possibility to wire an operational amplifier as a constant current source, or use transistor circuits. Nevertheless for designs with low quantities, there are ICs which can be used as current sources directly. The LM234, for example, is a voltage-controlled three-pin IC, providing a current with a maximum error of 0.1 %/V change in the supply voltage. The maximum current provided is 10 mA, which is usually sufficient for the supply of optical or resistive sensors.

The change of the signal is usually measured in relation to a voltage in the system. In this case, it is necessary to provide a voltage which is very well known and independent from temperature effects or changes of the supply voltage. Common voltage regulators as used for electronic supply are not precise enough to fulfill these requirements. An alternative is given by Zener diodes operated in reverse direction. Such diodes, however, are not applicable to high loads and are of course only available in the steps of Zener voltages. Alternatively, reference voltage sources are available in many voltage steps on the market. The REF02, for example, is a six-pin IC, providing a temperature-stable voltage of 5 V with an error of 0.3 %. The drivable load of such voltage sources is limited, in case of the REF02 it is 10 mA, but this is usually not a relevant limit as they are not thought as a supply to a complex circuit but only as a reference.

Compensation of Noise

The obvious solution for the compensation of noise in a measurement signal is given by the usage of a carrier frequency for modulating the signal. A prerequisite of course is given by the sensor showing no damping at the modulating frequency. This is usually no problem for optical sensors in the range of several kilohertz. At the receiver, the signal is bandpass-filtered and equalized or otherwise averaged. This suppresses disturbance frequencies or otherwise superimposed offsets.

A simple but very effective circuit for noise compensation is the use of so-called lock-in amplifiers. On the side of the sender, a signal is switched between the states *on* and *off* at a frequency f. In the receiver, the wanted signal such as, e.g., the offset and other disturbing frequencies are received. A following amplifier is switched with the same frequency between $+1$ and -1 in such a way, that with the receipt of the wanted signal including the disturbance the positive amplification happens. During the period without the wanted signal, when the receiver measures the disturbance only, the signal is inverted with -1. The resulting signal is low-pass filtered afterward, resulting in a subtraction of the noise signal and providing a voltage proportional to the wanted signal only.

10.2.7 Acceleration and Velocity Measurement

Beside the direct position measurement, haptic systems sometimes demand some knowledge about the first or second derivative of position in form of velocity or acceleration. Such a necessity may be given with stability issues for closed-loop systems or impedance behavior of users or manipulated objects. The acquisition can either be done by direct measurement or by differentiation of the position-signal with digital or analog circuits. Additionally, it can be imagined to, e.g., measure velocity and calculate the position by integration. The capabilities of integration and differentiation and their limits, such as typical direct measurement principles, are sketched in this section.

10.2.7.1 Integration and Differentiation of Signals

The integration and differentiation of signals can either be done analog or digital. Both variants have different advantages and disadvantages.

Analog Differentiation

The basic circuit for an active analog integrator is shown in Fig. 10.49a. It is a high-pass filter, which already gives hints on the challenges connected with differentiation. The high-pass behavior is limited in its bandwidth. The upper border frequency is given by the resonance frequency $f_R = \frac{1}{2\pi RC}$ and by the bandwidth of the operational amplifier. As these components are sufficiently dynamic for haptic applications, this should be no problem in practical realization. Due to the negative feedback, however, the natural bandwidth limit of the operational amplifier at high frequencies has a phase of 90° adding to the phase of 90° from the differentiation. This makes the circuit sensitive to become electrically instable and oscillate [96].

This effect can be compensated by a serial resistance with a capacity C, which is identical to a linear amplification with the operational amplifier. This diminishes the phase for high frequencies by 45° resulting in a phase margin to the instable border condition. Analog differentiation is an adequate method for the derivation of velocities from positioning signals. A double analog differentiation needs a careful design of the corresponding circuit, as a number of capacitive inputs are placed in series. Additionally, it should be considered that the amplitude of the operational amplifier is limited by the supply voltage. Accordingly, the amplitude's dynamic has to be adjusted to the maximum signal change expected.

Analog Integration

The basic circuit of an active analog integrator is given in Fig. 10.49b. Analog integration is a reliable method from analog calculation technique, but has limited use for haptic applications. The circuit has an upper border frequency given by the resonance $f_R = \frac{1}{2\pi RC}$, and for a nonideal operational amplifier, it has a lower border frequency

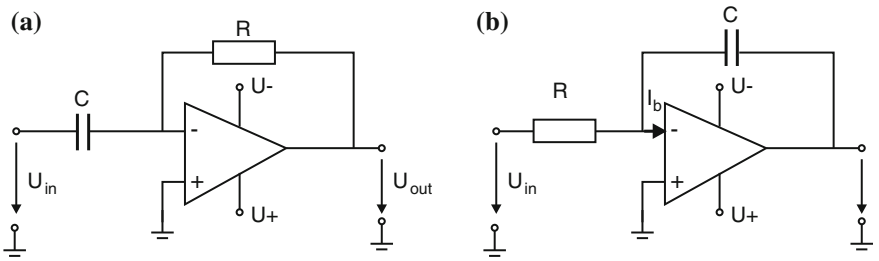

Fig. 10.49 Analog circuits for **a** differentiation and **b** integration [96]

too. This is a result of the current I_b at the input of the OP-amplifier charging the capacitor with $U_{\text{in}} = 0$ V continuously. If $C = 10\,\mu$F and $I_b = 1\,\mu$A, the voltage increases by 0.1 V per second. Whereas in signal processing applications, this can be compensated by high-passes in series, for haptic applications covering a bandwidth from several seconds to 10 kHz this behavior is usually not acceptable.

Digital Differentiation

Digital differentiation is realized by a subtraction of two consecutive measurement values. It is very applicable, especially when the signal is measured at high frequencies. The quality of the signal is dependent on the noise on the input. Frequently, the least-significant bit of, e.g., an AD-conversion is rejected before the differentiation is performed, as it is oscillating with the noise of the AD-conversion (quantization-noise). To derive velocity from position measurements, COLGATE recommends a high-position measurement resolution as well as a low-pass filtering of the generated velocity signal to improve the quality [17].

Digital Integration

Digital integration is the summation of continuous measurement values and the division of the sum by the number of values. Alternatively, it can be the sum of discrete changes of a measurement value. The incremental measurement of a digital encoder is also a form of integration on the basis of change information. The procedure is robust at high frequencies beyond the actual upper border frequency of the signal. Beside a sufficient dimension of the register size for the measurement values to prevent an overflow, there is nothing else to worry about.

10.2.7.2 Induction as a Velocity Measure

The most frequent variant to gain information about velocity is given by the digital signal processing of a position measurement. Nevertheless to be able to measure velocity directly, the use of a velocity-proportional physical effect is mandatory. Beside Doppler-ultrasonic measurement, which is seldom applicable to haptic systems due to the wavelengths (compare Sect. 10.2.6), the use of electrical induction is the most frequently used direct effect. Accordingly, an electrical-induced voltage U is generated in a conductor of the length l, moving orthogonal in a magnetic field B with the velocity v:

$$U = v\,B\,l. \tag{10.44}$$

Special geometric designs as given with electrodynamic actuators (Sect. 9.2) can be used for velocity measurements with inducing voltages in their coils. In contrast to electrodynamic actuators, the design requires a maximization of conductor length, to generate a pronounced voltage signal. The inductivity of the winding generates a low-

pass characteristic in combination with its own resistance. This limits the dynamic of the signal. The biggest error made with these kinds of sensors is given by a bad homogeneity of the winding due to dislocation of single turns. This manufacturing error results in different winding lengths moving in the B-field at different positions of the sensor, which is directly affecting the quality of the measured signal.

10.2.7.3 Force Sensors as Acceleration Sensors

In contrast to velocity measurement, to measure accelerations a wide variety of sensors exists. Ignoring some exceptions, most of them are based on the relation

$$\mathbf{a} = \frac{\mathbf{F}}{m}. \tag{10.45}$$

In fact, the force measurement principles given in Sect. 10.1 are added by a known mass m only, resulting in a mechanical strain of a bending element or generating another acceleration-proportional signal. In professional measurement technology especially piezoelectric sensors for high-dynamic measurements, but also piezoresistive sensors for low-frequency accelerations are established. In mechatronic systems with high quantities, micromechanical acceleration sensors with comb-like structures in silicon according to the capacitive measurement principle are used. The requirements of automotive industry for airbags and drive stability programs to measure acceleration in many directions made low-price and robust ICs available at the free market, e.g., the ADXL series of Analog Devices. The bandwidth of these sensors ranges from 400 Hz to 2.5 kHz with maximum accelerations >100 g in up to three spatial directions. Only a wide variance of their characteristic values, e.g., the output voltage at 0 g, requires a calibration of the individual sensor.

10.2.8 Conclusion on Position Measurement

With haptic devices, position measurement is a subordinated problem. In the range of physiological perceived displacements resolutions, there are enough sensor principles which are sufficiently precise and dynamic for position measurement. The calculation or measurement of accelerations or velocities is easily possible too. Without doubt, the optical measurement technology is the most frequently used technical solution. Nevertheless especially for the design of specific actuators it is indicated to ask the questions, whether there are other sensor principles applicable for a direct integration into the actuator.

If there are specific requirements for measurement in the range of a few μm positioning resolution, the proposed principles should be treated with reserve. Measurements in the range of μm require specific optical or capacitive measurement technology. With the exception of special psychophysical questions, it is unlikely that such requirements are formulated for haptic devices.

10.3 Touch Sensors

Christian Hatzfeld

With the increasing number of systems using touch-sensitive surfaces for ↪HCI, touch sensors have become more prevalent. They detect whether a human user touches a sensitive two- or three-dimensional surface of an object or system. One can differentiate between sensors that detect the contact position and ones that detect different types of touch or contact pose.

When analyzing this kind of systems, one can identify several functional principles. Because of robustness, low costs, and high sensitivity, resistive and capacitive principles are among the most used in ↪HCI. DAHIYA AND VALLE provide a thorough analysis of different measurement principles in [19] for the usage in robotic applications. In the following, the function of resistive and capacitive systems is described in more detail.

10.3.1 Resistive Touch Sensors

Resistive touch sensors to detect contact positions are based on two flexible, conductive layers that are normally separated from each other. If a user touches one of the layers, a connection is made between both layers and the position of the connection point can be calculated from the different resistances as shown in Fig. 10.50 based on Eqs. 10.46 and 10.47.

$$u_{\mathrm{x,out}} = \left.\frac{R_2}{R_1 + R_2} U_{x1}\right|_{U_{x2} = 0\mathrm{V},\quad U_{y3}, U_{y4} \text{ in Hi-Z state}} \tag{10.46}$$

$$u_{\mathrm{y,out}} = \left.\frac{R_4}{R_3 + R_4} U_{y3}\right|_{U_{y4} = 0\mathrm{V},\quad U_{x1}, U_{x2} \text{ in Hi-Z state}} \tag{10.47}$$

Resistive touch sensors exhibit a high resolution of up to 4,096 dpi in both dimensions and a high response speed (<10 ms). With additional wiring, the pressure on the screen also can be recorded. This principle does not support multitouch detection, i.e., the simultaneously contact in more than one position, with the setup shown in Fig. 10.50. A simple mean to measure multitouch interaction, too, is the segmentation of one of the conductive layers in several (n) conductive strips called *hybrid analog resistive touch sensing*. This increases the number of calculations to obtain a position reading from 2 to $2n$, but this is still less than the calculation of a whole matrix with at least n^2 calculations.

For the usage of resistive touch sensors, there are a couple of commercially available integrated circuits (as for example MAX 11800 with a footprint as low as 1.6×2.1 mm^2) that will alleviate the integration of such a sensor in a new system.

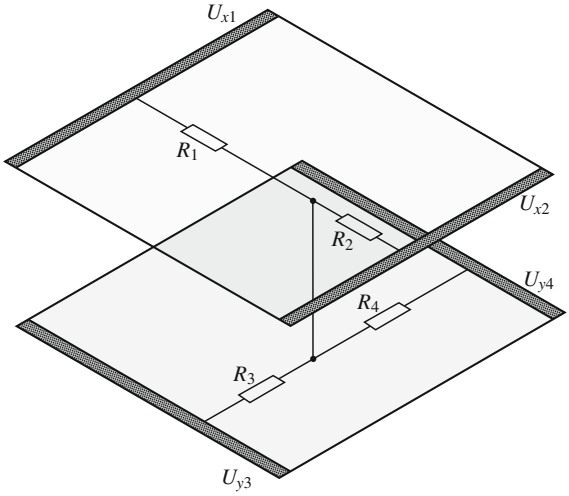

Fig. 10.50 Principle of resistive touch sensors

10.3.2 Capacitive Touch Sensors

For capacitive touch sensors' detecting positions, two general approaches are known. *Self-capacitance* or *surface-capacitance* sensors are built up from a single electrode. The system measures the capacitance to the environment that is altered when a user touches the surface. Based on the measurement of the current that is used to load the changed capacitance, a position measure can be deducted similar to the calculation in the case of resistive sensors. This sensor type is prone to errors from parasitic capacitive coupling, the calculation of multiple touch positions is possible but requires some effort.

When more than one capacitor is integrated in a surface, one can use the mutual capacitance type sensor. In that case, the capacitors are arranged in a matrix and the capacitance of each capacitor is changed by approaching conductive materials like fingers or special styluses. This matrix is read out consecutively by the sensor controller. Because of the matrix arrangement, the detection of multipoint touch is possible. As with resistive sensor systems, there are several commercially available integrated circuits for the readout of such capacitive matrices.

For the identification of contact poses, for example, the touch with a single finger or a whole hand, the self-capacitance approach can be used as well. In that case, the changed capacitance is considered as an indicator for the touch pose with regard to an arbitrary-shaped electrode. Since the realization of such a function is quite simple in terms of the required electronics, this procedure is incorporated in standard components under several brand names, like, for example, ATMEL QTOUCH.

Sometimes, capacitive sensor systems are combined with inductive sensor systems that track the position of a coil with respect to the reference surface. This is for example used to make use of stylus' on touchscreens and graphic tablets. Because of the different sensor principles, one can weigh the tool equipped with the coil more and avoid misreadings by the capacitive effect of the user's hand.

Table 10.6 Advantages and disadvantages of different touch-sensing principles according to [19]

Sensing principle	Advantages	Disadvantages
Capacitive	Sensitive, low cost, commercial readout circuits available	Cross-talk, hysteresis, complex electronic
Conductive composites	Mechanically flexible, easy fabrication, low cost	Hysteresis, nonlinear response, slow reaction time
Magnetic	High sensitivity, good dynamic range, no mechanical hysteresis, robust	Restricted to nonmagnetic medium, complex readout, size, high power consumption
Optical	Sensitive, immune to electromagnetical interference, no electrically conductive parts, flexible, fast response	Bulky, sensitive to bending, power consumption, complex readout
Piezoelectric	High sensitivity, good dynamic response, high bandwidth	Temperature sensitive, difficult electrical connection, no static measurement
Piezoresistive	High sensitivity, low cost, low noise, simple electronics	Mechanically stiff, nonlinear, hysteresis, signal drift
Resistive	High sensitivity, low cost, commercial readout circuits available	Power consumption, no multitouch, no contact-force measurement
Ultrasonic	Fast dynamic response, good force resolution	Limited utility at low frequency, temperature sensitive, complex electronics

10.3.3 Other Principles

However, a lot of other principles are known as well, that are often based on the change of a position and a detection of this change with different sensing principles. Examples include optical and magnetic measuring principles as described above in Sect. 10.2. They are often investigated in the context of robot tactile sensing, where not only touch, but also pose, handling, and collision are of interest [19].

In these cases, the use of flexible materials and microtechnology is of interest, which makes this kind of sensor to be the most welcomed examples for microsystem engineers. For the use in haptic systems, the current state of development of such systems as, for example, shown in [19, 27, 95] has to be critically checked. As a general classification, Table 10.6 gives some advantages and disadvantages for possible sensing principles.

A last example for advanced touch sensors shall be given: Based on an impedance spectroscopy measurement, the TOUCHÉ system by SATO ET AL. allows to differentiate different grips and body poses from an impedance measurement. Examples include the identification of the finger positions on a door knob, the discrimination of arm poses when sitting on a table or even the detection of someone touching a water surface. Applications include gesture interfaces for worn and integrated computers as well as the possibility of touch passwords, that consist out of a predefined sequence of touch poses [80].

10.4 Imaging Sensors

Within the contents of this book, the focus is laid on device-based sensors, like the above-described sensors for force, deflection, and touch. Pure input sensors, such as the imaging sensors, will be not discussed further as per definition no haptic feedback can be given without a real physical contact. Nevertheless, they can be used to build a complex HMI when combined with body-worn tactile devices and should be kept in mind for such applications. For that purpose, one can differentiate two general classes of imaging sensors:

1. *Direct imaging sensors* are usually based on camera systems observing the user or body parts, deriving commands from gestures performed with extremities or facial expressions. Such imaging systems are subject to application in controlled environments (such as inside a car), for direct computer or gameplay interaction (*Microsoft* XBOX KINECT), or even touch interaction on surfaces
2. *Marker-based imaging senors* are again based on camera systems observing special markers worn or held by the user. Such systems can be highly accurate due to the knowledge of relations between markers and their sizes. They are used in professional navigation application such as surgical applications or motion-capture technologies and can also be found in gameplay situation such as the *Sony* PLAYSTATION MOVE CONTROLLER.

10.5 Conclusion

With the exception of force/torque sensors, commercially available sensors for position, velocity, acceleration, touch, and images exhibit sufficient properties for the usage in haptic systems. Within this section, the necessary knowledge of the underlying sensing principles for sound selection from available sensors is reported. For the use of force/torque sensors, the relevant principle and design steps for the development of a customized sensor are given and can be deepened in the below-mentioned background readings.

Recommended Background Reading

[6] Barlian, A. & Park, W. & Mallon, J. & Rastegar, A. & Pruitt, B.: **Review: Semiconductor Piezoresistance for Microsystems**. Proceedings of the IEEE 97, 2009.
Review on piezoresistive silicon sensors. Physics, examples, sensor characteristics.

[11] Bray, A. & Barbato, G. & Levi, R.: **Theory and practice of force measurement**. Monographs in physical measurement, Academic Press Inc., 1990.
Discussion of examples of force sensors. Basic mechanics and hints for designing deformation elements.

[19] Dahiya, R. S. & Valle, M.: **Robotic Tactile Sensing**, Springer, 2013.
Overview about sensing principles used for robotic applications that are also usable for haptic systems.

[35] Keil, S.: **Beanspruchungsermittlung mit Dehnungsmessstreifen**. Cuneus Verlag, 1995.
All about strain gages. History, materials and technology, selection and application.

[47] Lenk, A. & Ballas, R.G. & Werthschützky, R.& Pfeifer, G.: **Electrical, Mechanical and Acoustic Networks, their Interactions and Applications**. Springer, 2011.
Introduction in modeling dynamics of electromechanical systems using network theory. Contains plenty of useful examples.

[72] Rausch, J.: **Entwicklung und Anwendung miniaturisierter piezoresistiver Dehnungsmesselemente**. Dr-Hut-Verlag, München, 2012.
Comparison of sensing principles for strain sensing with focus on piezoresistive silicon elements. Design of a tri-axial force sensor using semiconducting strain gages.

[98] Tränkler H.R.& Obermeier, E.:**Sensortechnik: Handbuch für Praxis und Wissenschaft**. Springer, 1998.
Extensive overview of sensors and sensor electronics.

[107] Young, W.C., Budynas, R.G.:**Roark's formulas for stress and strain. Bd. 6.** McGraw-Hill, New York, 2002
Mechanics Handbook for calculation of stress and strain fields in complex deformation bodies.

References

1. Amor A, Budde T, Gatzen H (2006) A magnetoelastic microtransformer-based microstrain gauge. Sens Actuators A Phys 129(1–2):41–44. doi:10.1016/j.sna.2005.09.043
2. Arshak K, McDonagh D, Durcan M (2000) Development of new capacitive strain sensors based on thick film polymer and cermet technologies. Sens Actuat A Phys 79(2):102–114. doi:10.1016/S0924-4247(99)00275-7
3. Arshak K et al (2006) Development of high sensitivity oxide based strain gauges and pressure sensors. J Mater Sci Mater Electron 17(9):767–778. doi:10.1007/s10854-006-0013-4
4. Ballas R (2007) Piezoelectric multilayer beam bending actuators: static and dynamic behavior and aspects of sensor integration. Springer, Berlin, pp XIV, 358. ISBN: 978-3-540-32641-0
5. Bao M-H (2004) Micro mechanical transducers: pressure sensors, accelerometers and gyroscopes, vol 8, 2nd edn. Handbook of sensors and actuators 8. Elsevier, Amsterdam, pp XIV, 378. ISBN: 9780080524030
6. Barlian A et al (2009) Review: semiconductor piezoresistance for microsystems. Proc IEEE 97(3):513–552. doi:10.1109/JPROC.2009.2013612
7. Berkelman P et al (2003) A miniature microsurgical instrument tip force sensor for enhanced force feedback during robot-assisted manipulation. IEEE Trans Rob Autom 19(5):917–921. doi:10.1109/TRA.2003.817526
8. Beyeler F et al (2007) Design and calibration of a MEMS sensor for measuring the force and torque acting on a magnetic microrobot. J Micromech Microeng IOP 18:025004 (2007). doi:10.1088/0960-1317/18/2/025004

9. Botsis J et al (2004) Embedded fiber Bragg grating sensor for internal strain measurements in polymeric materials. Opt Lasers Eng 43. doi:10.1016/j.optlaseng.2004.04.009
10. Brand U, Büttgenbach S (2002) Taktile dimensionelle Messtechnik für Komponenten der Mikrosystemtechnik. In: tm-Technisches Messen/Plattform für Methoden. Systeme und Anwendungen der Messtechnik 12. doi:10.1524/teme.2002.69.12.542
11. Bray A, Barbato G, Levi R (1990) Theory and practice of force measurement. Monographs in physical measurement. Academic Press Inc., Waltham. ISBN: 978-0121284534
12. Burdea GC (1996) Force and touch feedback for virtual reality. Wiley-Interscience, New York
13. Caldwell DG, Lawther S, Wardle A (1996) Multi-modal cutaneous tactile feedback. In: Proceedings of the IEEE international conference on intelligent robots and systems. Diss, pp 465–472. doi:10.1109/IROS.1996.570820
14. Calvert P et al (2007) Piezoresistive sensors for smart textiles. Electroact Polym Actuators Devices (EAPAD) 2007:65241i-8. doi:10.1117/12.715740
15. Chase T, Luo R (1995) A thin-film flexible capacitive tactile normal/shear force array sensor. In: Proceedings of the 1995 IEEE IECON 21st international conference on industrial electronics, control, and instrumentation, vol 2. Orlando, FL, pp 1196–1201. doi:10.1109/IECON.1995.483967
16. Cochrane C et al (2007) Design and development of a flexible strain sensor for textile structures based on a conductive polymer composite. Sensors 7(4):473–492. doi:10.3390/s7040473
17. Colgate J, Brown J (1994) Factors affecting the Z-Width of a haptic display. In: Proceedings of IEEE international conference on robotics and automation, vol 4, pp 3205–3210. doi:10.1109/ROBOT.1994.351077
18. Cranny A et al (2005) Thick-film force, slip and temperature sensors for a prosthetic hand. Measur Sci Technol IOP 16:931–941. doi:10.1016/j.sna.2005.02.015
19. Dahiya RS, Valle M (2013) Robotic Tactile Sensing. Springer, Berlin. doi:10.1007/978-94-007-0579-1
20. Kurtz AD (1962) Adjusting crystal characteristics to minimaze temperature dependency. In: Dean M, Douglas RD (eds) Semiconductor and conventional strain gages. Academic Press Inc. New York, ISBN: 978-1114789906
21. Dölle M (2006) Field effect transistor based CMOS stress sensors. PhD thesis. IMTEK, University of Freiburg. ISBN: 978-3899594584
22. Ferdinand P et al (1997) Applications of bragg grating sensors in Europe. In: International conference on optical fiber sensors OFS. Wiliamsburg, Virginia. ISBN: 1-55752-485-8
23. First Sensor Technology GmbH (2009) T-Brücke. Technical report. First Sensor Technology GmbH. http://www.first-sensor.com/
24. Fung Y-C (1993) Biomechanics: mechanical properties of living tissues, 2nd edn. Springer, New York, pp XVIII, 568. ISBN: 0-387-97947-6; 3-540-97947-6
25. Gall M, Thielicke B, Poizat C (2005) Experimentelle Untersuchungen und FE-Simulation zum Sensor-und Aktuatoreinsatz von flächigen PZT-Funktionsmodulen. In: Deutsche Gesellschaft fürMaterialkunde e.V. http://publica.fraunhofer.de/dokumente/N-28844.html
26. Gehin C, Barthod C, Teissyre Y (2000) Design and characterization of new force resonant sensor. Sens Actuat A Phys 84: 65–69. doi:10.1016/S0924-4247(99)00359-3
27. Goethals P (2008) Tactile feedback for robot assisted minimally invasive surgery: an overview. Technical report workshop, Eurohaptics conference. Department of Mechanical Engineering, K.U. Leuven
28. Gross D et al (2009) Technische Mechanik: Band 2: Elastostatik. Springer, Berlin. ISBN: 978- 3540243120
29. Hagedorn P et al (1998) The importance of rotor flexibility inultrasonic traveling wave motors. Smart MaterStruct 7:352–368. doi:10.1088/0964-1726/7/3/010
30. Hasegawa Y, Shikida M et al (2006) An active tactile sensor for detecting mechanical characteristics of contacted objects. J Micromech Microeng IOP 16:1625–1632. doi:10.1088/0960-1317/16/8/026
31. Hasser CJ, Daniels MW (1996) Tactile feedback with adaptive controller for a force-reflecting haptic display—Part I: design. In: Proceedings of the fifteenth southern biomedical engineering conference, pp 526–529. doi:10.1109/SBEC.1996.493294

32. Hoffmann K (1985) Eine Einführung in die Technik des Messens mit Dehnungsmessstreifen. Hottinger Baldwin Messtechnik GmbH (HBM)
33. Hou L (1999) Erfassung und Kompensation von Fehlereffekten bei der statischen Kraftmessung mit monolithischen Nd:YAG-Laserkristallen. PhD thesis, Universität Kassel. https://kobra.bibliothek.uni-kassel.de/handle/urn:nbn:de:hebis:34-159?mode=full
34. Inaudi D (2004) SOFO sensors for static and dynamic measurements. In: 1st FIG international symposium on engineering surveys for construction works and structural engineering. Nottingham. http://cordis.europa.eu/result/report/rcn/41123_en.html
35. Keil S (1995) Beanspruchungsermittlung mit Dehnungsmessstreifen. Cuneus Verlag. ISBN: 978- 3980418805
36. Kerdok A (2006) Characterizing the nonlinear mechanical response of liver to surgical manipulation. PhD thesis, Harvard University, Cambridge. URL: http://biorobotics.harvard.edu/pubs/akthesis.pdf
37. Kern T (2006) Haptisches Assistenzsystem für diagnostische und therapeutische Katheterisierungen. PhD thesis, Techische Universität Darmstadt, Institut für Elektromechanische Konstruktionen. http://tuprints.ulb.tu-darmstadt.de/761/
38. Kersey A et al. (1997) Fiber grating sensors. J Lightwave Technol 15(8). doi:10.1109/50.618377
39. Kim K et al (2007) Calibration of multi-axis MEMS force sensors using the shape-from-motion method. IEEE Sens J 7(3):344–351. doi:10.1109/JSEN.2006.890141
40. Kizilirmak G (2007) Frei applizierbare MOSFET-Sensorfolie zur Dehnungsmessung". PhD thesis, RWTH Aachen. http://darwin.bth.rwth-aachen.de/opus3/volltexte/2007/1973/pdf/Kizilirmak_Goekhan.pdf
41. Klages S (2004) Neue Sensorkonzepte zur Zungendruckmessung. Diplomarbeit, Darmstadt: Technische Universität Darmstadt, Institut für Elektromechanische Konstruktionen. http://tubiblio.ulb.tu-darmstadt.de/53658/
42. Kon S, Oldham K, Horowitz R (2007) Piezoresistive and piezoelectric MEMS strain sensors for vibration detection. In: Proceedings of SPIE, vol 6529, p 65292V-1. doi:10.1117/12.715814
43. Kunadt A et al (2010) Messtechnische Eigenschaften von Dehnungssensoren aus Kohlenstoff-Filamentgarn in einem Verbundwerkstoff. In: tm-TechnischesMessen/Plattform fürMethoden, Systeme und Anwendungen der Messtechnik 77(2):113–120. doi:10.1524/teme.2010.0014
44. Lang U et al (2009) Piezoresistive properties of PEDOT: PSS. Microelectron Eng 86(3):330–334. doi:10.1016/j.mee.2008.10.024
45. LaserComponents Group (2008) Faseroptische Sensoren. http://www.lasercomponents.com/de/1134.html
46. Latessa G et al (2009) Piezoresistive behaviour of flexible PEDOT.PSS based sensors. Sens Actuat B Chem 139(2):304–309. DOI:http://dx.doi.org/10.1016/j.snb.2009.03.063
47. Lenk A et al (ed) (2011) Electromechanical systems in microtechnology and mechatronics: electrical, mechanical and acoustic networks, their interactions and applications. Springer, Heidelberg
48. Luo F et al (1999) A fiber optic microbend sensor for distributed sensing application in the structural strain monitoring". Sens Actuat A Phys 75:41–44. doi:10.1016/S0924-4247(99)00043-6
49. Maiwald M et al (2010) INKtelligent printed strain gauges. Sens Actuat A Phys 162(2):198–201. doi:10.1016/j.sna.2010.02.019
50. Matsuzaki R, Todoroki A (2007) Wireless flexible capacitive sensor based on ultra-flexible epoxy resin for strain measurement of automobile tires. Sens Actuat A Phys 140(1):32–42. doi:10.1016/j.sna.2007.06.014
51. Mehner J (2000) Entwurf in der Mikrosystemtechnik, vol 9. Dresdner Beiträge zur Sensorik. Dresden University Press. ISBN 9783931828479
52. Meiss T et al (2007) Fertigung eines Miniaturkraftsensors mit asymmetrischem Grundkrper zur Anwendung bei Katheterisierungen. In: MikroSystemTechnik. https://www.vde-verlag.de/proceedings-de/563061014.html

53. Meiss T (2012) Silizium-Mikro-Kraftsensoren für haptische Katheterisierungen: Entwurf, Musterbau und Signalverarbeitung sowie erste Validierung des Assistenzsystems HapCath. PhD thesis, Technische Universität Darmstadt, Institut für Elektromechanische Konstruktionen. http://tuprints.ulb.tu-darmstadt.de/2952/
54. Meißner P (2007) Optische Nachrichtentechnik I—Skriptum zur Vorlesung. Skriptum
55. Meißner P (2006) Seminar zu speziellen Themen der optischen Nachrichtentechnik—Simulatorische und experimentelle Untersuchungen optischer WDM Übertragungssysteme. Skriptum
56. Meschede D (2007) Optics, light and lasers: the practical approach to modern aspects of photonics and laser physics. 2nd edn. Optik, Licht und Laser engl. Weinheim: Wiley-VCH-Verlag, pp IX, 560. ISBN: 978-3-527-40628-9
57. Michel J (1995) Drehmomentmessung auf Basis funkabfragbarer Oberflächenwellen-Resonatoren. PhD thesis, Technische Universität München. http://www.mst.ei.tum.de/forschung/veroeffentlichungen/abgeschlossene-dissertationen.html
58. Micron Instruments (2012) U-shaped semiconductor gage. http://www.microninstruments.com/
59. Müller M (2009) Untersuchungen zu Kraft-Momenten-Sensoren auf Basis von Faser-Bragg-Gittern. PhD thesis, Technische Universität München. https://mediatum.ub.tum.de/doc/956469/956469.pdf
60. Nakatani M, Howe R, Tacji S (2006) The fishbone tactile illusion. In: Eurohaptics. IEEE. Paris. http://lsc.univ-evry.fr/eurohaptics/upload/cd/papers/f46.pdf
61. Nührmann D (1998) Das große Werkbuch Elektronik, vol 7. Franzis' Verlag, Poing. ISBN: 3772365477
62. Oddo C et al (2007) Investigation on calibration methods for multi-axis, linear and redundant force sensors. Measur Sci Technol 18:623. doi:10.1088/0957-0233/18/3/011
63. Palais JC (2005) Fiber optic communications, 5th edn. Pearson Prentice-Hall, Upper Saddle River, pp XIII, 441. ISBN: 0130085103
64. Pandey N, Yadav B (2006) Embedded fibre optic microbend sensor for measurement of high pressure and crack detection. Sens Actuat A Phys 128:33–36. doi:10.1016/j.sna.2006.01.010
65. Partsch U (2002) LTCC-kompatible Sensorschichten und deren Applikation in LTCC-Drucksensoren, 1st edn, vol 9. Elektronik-Technologie in Forschung und Praxis 9. Templin/Uckermark: Detert, pp III, 163. ISBN: 3934142117
66. Pasquale M (2003) Mechanical sensors and actuators. Sens Actuat A Phys 106(1–3):142–148. doi:10.1016/S0924-4247(03)00153-5
67. Peirs J et al (2004) A micro optical force sensor for force feedback during minimally invasive robotic surgery. Sens Actuat A Phys 115(2–3):447–455. doi:10.1016/j.sna.2004.04.057
68. Pfeifer G, Werthschützky R (1989) Drucksensoren. Verlag Technik. ISBN: 978-3341006603
69. Physik Instrumente (PI) GmbH (2010) Flächenwandlermodul. http://www.physikinstrumente.de/de/produkte/prdetail.php?sortnr=101790
70. Ping L, Yumei W (1996) An arbitrarily distributed tactile sensor array using piezoelectric resonator. In: Instrumentation and measurement technology conference IMTC-96. IEEE conference proceedings, vol 1. Brussels, pp 502–505. doi:10.1109/IMTC.1996.507433
71. Puers R (1993) Capacitive sensors: when and how to use them. Sens Actuat A Phys 37–38:93–105. doi:10.1016/0924-4247(93)80019-D
72. Rausch J (2012) Entwicklung und Anwendung miniaturisierter piezoresistiver Dehnungsmesselemente. Dissertation, Technische Universität Darmstadt. http://tuprints.ulb.tudarmstadt.de/3003/1/Dissertation-Rausch-online.pdf
73. Rausch J et al (2006) INKOMAN-Analysis of mechanical behaviour of liver tissue during intracorporal interaction. In: Gemeinsame Jahrestagung der Deutschen, Österreichischen und Schweizerischen Gesellschaften für Biomedizinische Technik 6(9)
74. Reindl L et al (2001) Passive funkauslesbare sensoren (wireless passive radio sensors). In: TM—Technisches messen/plattform für methoden, Systeme und anwendungen der Messtechnik 68(5):240. doi:10.1524/teme.2001.68.5.240

75. Rey P, Charvet P et al (1997) A high density capacitive pressure sensor array for fingerprint sensor application. In: International conference on solid-state sensors and actuators, IEEE. Chicago. doi:10.1109/SENSOR.1997.635738
76. Rosen J, Solazzo M, Hannaford M (2002) Task decomposition of laparoscopic surgery for objective evaluation of surgical residents learning curve using hidden markov model. In: computer aided surgery 7. http://www.ncbi.nlm.nih.gov/pubmed/12173880
77. Roths J, Kratzer P (2008) Vergleich zwischen optischen Faser-Bragg-Gitter-Dehnungssensoren und elektrischen Dehnungsmessstreifen. In: TM-Technisches Messen 75(12), pp 647–654. doi:10.1524/teme.2008.0903
78. Russell R (1992) A tactile sensory skin for measuring surface contours. In: Tencon 1992 region 10 conference. IEEE, Melbourne. doi:10.1109/TENCON.1992.271943
79. Saraf R, Maheshwari V (2006) High-resolution thin-film device to sense texture by touch. Technical report 5779, pp 1501–1504. http://www.sciencemag.org/content/312/5779/1501.full
80. Sato M, Poupyrev I, Harrison C (2012) Touché: enhancing touch interaction on humans, screens, liquids, and everyday objects. In: Proceedings of the 2012 ACMannual conference on human factors in computing systems, pp 483–492. doi:10.1145/2207676.2207743
81. Schaumburg H (1992) Sensoren, vol 3. Werkstoffe und Bauelemente der Elektrotechnik 3. Stuttgart: Teubner Verlag, p 517. ISBN: 3519061252
82. Schlüter V (2010) Entwicklung eines experimentell gestützten Bewertungsverfahrens zur Optimierung und Charakterisierung der Dehnungsübertragung oberflächenapplizierter Faser-Bragg-Gitter- Sensoren. PhD thesis, Bundesanstalt für Materialforschung und -prüfung - BAM. http://www.bam.de/de/service/publikationen/publikationen_medien/dissertationen/diss_56_vt.pdf
83. Schreier-Alt T (2006) Polymerverkapselung mechatronischer Systeme—Charakterisierung durch eingebettete Faser Bragg Gitter Sensoren". PhD thesis, Technische Universität Berlin, Fakultät IV - Elektrotechnik und Informatik. http://opus4.kobv.de/opus4-tuberlin/frontdoor/index/index/docId/1494
84. Sektion für UT (1999) Minimal Invasive Chirurgie Tübingen. Verbundprojekt TAMIC—Entwicklung eines taktilen Mikrosensors für die Minimal Invasive Chirurgie - Schlussbericht. Technical report. https://www.yumpu.com/de/document/view/6617211/verbundprojekttamic-entwicklung-eines-taktilen-experimentelle-
85. Sergio M et al (2003) A dynamically reconfigurable monolithic CMOS pressure sensor for smart fabric. IEEE J Solid-State Circ 38(6):966–968. doi:10.1109/JSSC.2003.811977
86. Simone C (2002) Modelling of neddle insertion forces of percutaneous therapies. Johns Hopkins University, Diplomarbeit. Baltimore. doi:10.1109/ROBOT.2002.1014848, http://ieeexplore.ieee.org/xpls/abs_all.jsp?arnumber=1014848&tag=1
87. Sirohi J, Chopra I (2000) Fundamental understanding of piezoelectric strain sensors. J Int Mater Syst Struct 11(4):246–257. doi:10.1106/8BFB-GC8P-XQ47-YCQ0
88. Silicon Microstructures Incooperated (SMI) (2008) Pressure Sensors Products. http://www.si-micro.com/pressure-sensor-products.html
89. Smith C (1954) Piezoresistance effect in germanium and silicon. Phys. Rev. Am Phys Soc 94(1):42–49. doi:10.1103/PhysRev.94.42
90. Stavroulis S (2004) Rechnergestützter Entwurf von piezoresistiven Silizium-Drucksensoren mit realem mechanischem Wandler. Dissertation, Technische Universität Darmstadt, Institut für Elektromechanische Konstruktionen. http://tuprints.ulb.tu-darmstadt.de/473/
91. Stockmann M (2000) Mikromechanische Analyse der Wirkungsmechanismen elektrischer Dehnungsmessstreifen. Institut für Mechanik der technischen Universiät Chemnitz. http://www.qucosa.de/recherche/frontdoor/?tx_slubopus4frontend[id]=urn:nbn:de:bsz:ch1-200000494
92. Su L, Chiang K, Lu C (2005) Microbend-induced mode coupling in a graded-index multimode fiber. Appl Opt 44(34). doi:10.1364/AO.44.007394
93. Sun Y et al (2002) A bulkmicrofabricated multi-axis capacitive cellular force sensor using transverse comb drives. J Micromech Microeng IOP 12:832–840. doi:10.1088/0960-1317/12/6/314

94. Suster M et al (2006) A high-performance MEMS capacitive strain sensing system. J Microelectromech Syst 15:1069–1077. doi:10.1109/JMEMS.2006.881489
95. Tegin J, Wikander J (2005) Tactile sensing in intelligent robotic manipulation—a Review. Ind Rob 32(1):64–70. doi:10.1108/01439910510573318
96. Tietze U, Schenk C (2002) Halbleiter-Schaltungstechnik, 12th edn. Springer, Berlin, pp XXV, 1606. ISBN: 3-540-42849-6
97. Toda K (1994) Characteristics of interdigital transducers for mechanical sensing and nondestructive testing. Sens Actuat A Phys 44(3):241–247. doi:10.1016/0924-4247(94)00809-4
98. Tränkler H, Obermeier E (1998) Sensortechnik: Handbuch für Praxis undWissenschaft. Springer, Berlin. ISBN: 978-3-642-29941-4
99. Unterhofer K et al (2009) CMOS Stressmesssystem zur Charakterisierung von Belastungen auf MEMS Bauteile. In: MikroSystemTechnik KONGRESS 2009. VDE VERLAG GmbH. https://www.vde-verlag.de/proceedings-en/453183009.html
100. Valdastri P et al (2005) Characterization of a novel hybrid silicon three-axial force sensor. Sens Actuat A Phys 123–124. In: Eurosensors XVIII 2004—The 18th European conference on Solid-State Transducers, pp 249–257. doi:10.1016/j.sna.2005.01.006
101. Vasarhelyi G, Adama M et al (2006) Effects of the elastic cover on tactile sensor arrays. Sens Actuat A Phys 132:245–251. doi:10.1016/j.sna.2006.01.009
102. Vasarhelyi G, Fodor B, Roska T (2007) Tactile sensing-processing—interface-cover geometry and the inverse-elastic problem. Sens Actuat A Phys 140:8–18. doi:10.1016/j.sna.2007.05.028
103. Vazsonyi E et al (2005) Three-dimensional force sensor by novel alkaline etching technique. Sens Actuat A Phys 123–124:620–626. doi:10.1016/j.sna.2005.04.035
104. Voyles R, Morrow J, Khosla P (1997) The shape from motion approach to rapid and precise force/- torque sensor calibration. Trans ASME-G-J Dyn Syst Measur Control 119(2):229–235. doi:10.1115/1.2801238
105. Werthschützky R (2007) Mess- und Sensortechnik - Band II: Sensorprinzipien. Vorlesungsskriptum
106. Werthschützky R, Zahout C (2003) Angepasste Signalverarbeitung für piezoresistive Drucksensoren. In: tm-Technisches Messen/Plattform für Methoden, Systeme und Anwendungen der Messtechnik, pp 258–264. doi:10.1524/teme.70.5.258.20043
107. Young W, Budynas R (2002) Roark's formulas for stress and strain, vol 6. McGraw-Hill, New York. ISBN: 007072542X
108. Ziemann O (2007) POF-Handbuch: optische Kurzstrecken-Übertragungssysteme, 2nd edn. Springer, Berlin, pp XXX, 884. ISBN: 978-3540490937
109. Zwicker TU ((1989) Strain sensor with commercial SAWR. Sens Actuat A Phys 17(1–2):235–239. doi:10.1016/0250-6874(89)80085-X